STRUCTURES AND PROPERTIES OF Al-BASED Al–Si–Ni NANOSTRUCTURES DEVELOPED BY MECHANICAL ALLOYING

A

THESIS SUBMITTED IN PARTIAL FULFILLMENT OF THE REQUIREMENT FOR THE AWARD OF DEGREE OF MASTER OF TECHNOLOGY

in

Metallurgical & Materials Engineering

By

PARTHA SUNDAR MOHAKUD

Roll No-207MM106

DEPARTMENT OF METALLURGICAL & MATERIALS ENGINEERING
NATIONAL INSTITUTE OF TECHNOLOGY, ROURKELA
May, 2009

STRUCTURES AND PROPERTIES OF Al-BASED Al–Si–Ni NANOSTRUCTURES DEVELOPED BY MECHANICAL ALLOYING

A

THESIS SUBMITTED IN PARTIAL FULFILLMENT OF THE REQUIREMENT FOR THE AWARD OF DEGREE OF MASTER OF TECHNOLOGY

in

Metallurgical & Materials Engineering

By

PARTHA SUNDAR MOHAKUD
Roll No-207MM106

Under the Supervision of

Dr. Suhrit. Mula

DEPARTMENT OF METALLURGICAL & MATERIALS ENGINEERING
NATIONAL INSTITUTE OF TECHNOLOGY, ROURKELA
May, 2009

National Institute of Technology
Rourkela

CERTIFICATE

This is to certify that the thesis entitled, "**Structure and properties of Al-based Al–Si–Ni nanostructures developed by mechanical alloying**" being submitted by **Mr. Partha Sundar Mohakud** to the **Metallurgical and Materials Engineering Department** at **National Institute of Technology, Rourkela**, for the degree of **Master of Technology,** is a record of bona fide research work carried out under my supervision and guidance.

The result presented in this thesis has not been submitted elsewhere for the award of any Degree or Diploma. This work, in my opinion, has reached the standard of fulfilling the requirements for the award of the degree of **Master of Technology** in accordance with the regulation of the Institute.

(Dr. Suhrit Mula)

Department of Metallurgical and Materials Engineering

National Institute of Technology, Rourkela-769008

Acknowledgement

With deep regards and profound respect, I avail this opportunity to express my deep sense of gratitude and indebtedness to **Dr. Suhrit Mula**, Metallurgical and Materials Engineering Department, NIT Rourkela, for introducing the present research topic and for his inspiring guidance, constructive criticism and valuable suggestions throughout in this research work. It would have not been possible for me to bring out this thesis without his help and constant encouragement.

I am sincerely thankful to **Dr B.B.Verma, Professor and Head, Metallurgical and Materials Engineering Department** for his advice and providing necessary facilities for my work.

I also express my sincere gratitude to **Prof. S.K. Pratihar and Prof. S Bhattacharya, Dept. of Ceramic Engineering** for their kind help to carry out some part of the present work.

I am very much thankful to **Prof. S.C. Mishra, Dept. of Metallurgical and Materials Engineering & Dr. B. Bhoi, IIMT, Bhubaneswar,** for their kind cooperation regarding TEM study.

I am very much thankful to **R. K. Patel, Head of Dept. of Chemistry** for his kind cooperation for characterization of my samples by FTIR.

I am also thankful to **Sri Udayanath Sahu & Sri Rajesh Pattnaik,** Metallurgical & Materials Engineering, Technical assistants, for their co-operation.

Special thanks to **friends, staff of my Department and my family members** for being so supportive and helpful in every possible way.

Partha Sundar Mohakud

Abstract

An attempt was made to synthesize Al-based Al− Si − Ni amorphous and/or nanostructures by mechanical alloying (MA). The Al−Si−Ni alloys containing 14 to 25 % Si and 8 to 25 % Ni was known to generate amorphous phase by rapid solidification processing. Elemental powders of Al, Si and Ni (purity Ni ≥ 99.8%, Al ≥ 99.7%, Si ≥ 98.5%) having an average particle size <70 μm were blended to obtain nominal composition of $Al_{75}Si_{15}Ni_{10}$, $Al_{70}Si_{20}Ni_{10}$, $Al_{65}Si_{25}Ni_{10}$, $Al_{70}Si_{15}Ni_{15}$, $Al_{65}Si_{20}Ni_{15}$, $Al_{78}Si_{14}Ni_{8}$ and $Al_{50}Si_{25}Ni_{25}$. Mechanical alloying was carried out in a Fritsch high energy planetary ball mill using Cr-steel grinding media at 300 *r.p.m.* up to 50 h. Toluene was used as the process control agent. The ball to powder weight ratio was maintained at 10:1. The microstructural characterization of the milled powder was followed by X-ray diffraction (XRD), scanning electron microscopy (SEM) and transmission electron microscopy (TEM). The particle size distribution of the 50 h milled samples was carried out using a nano zeta sizer (NZS). Percentage transmittance of the milled sample was evaluated using Fourier transform infrared spectroscopy (FTIR). Partial amorphous structure was obtained in $Al_{75}Si_{15}Ni_{10}$ and $Al_{70}Si_{20}Ni_{10}$, whereas, Al-rich solid solution was observed in $Al_{65}Si_{25}Ni_{10}$, $Al_{70}Si_{15}Ni_{15}$ and $Al_{65}Si_{20}Ni_{15}$. Predominantly crystalline structure with intermetallic phases was observed in terminal compositions of $Al_{78}Si_{14}Ni_{8}$ and $Al_{50}Si_{25}Ni_{25}$. SEM micrographs showed that the powder morphology was changed from coarse layered structure obtained by very short period of milling to finer as the milling time increased. XRD and energy dispersive X-ray analysis (EDX) showed the formation of a homogeneous phase for all the compositions after milling for 50 h. The crystallite size, lattice microstrain (%) and lattice parameter were analyzed from major Al-peaks of the Al-rich solid solution. The crystallite size decreased very rapidly up to 10 h of milling and then became nearly constant (15-35 nm) with further milling, whereas, lattice microstrain (%) increased gradually up to 10 h very rapidly and then became nearly constant (0.5-0.6 %) with progress of milling. The variation of crystallite size and lattice microstrain (%) of Al-rich solid solutions with milling was found to be similar whereas, variation of lattice parameter of the Al-rich solid solutions was different. The

variation of lattice parameter with progress of milling possibly plays an important role in the amorphous phase formation by mechanical alloying.

Keywords: Amorphous; Nanostructures; X-ray diffraction (XRD); Transmission electron microscopy (TEM), nano zeta sizer (NZS), Fourier transform infrared ray (FTIR).

LIST OF FIGURES

LIST OF TABLES

CONTENTS

CHAPTER 1 Introduction

1.1 Al-based amorphous alloy

Aluminum based amorphous alloys find wide applications in aerospace, defence, automotive and transport industries due to their high strength to weight ratio, large elastic limit, lower elastic modulus, excellent wear and corrosion resistance [1]. The Performance of lightweight materials should be improved in order to fulfill the requirements and challenges like greater efficiency, reduced emissions and environmental impact of the aerospace, defence and automotive industries. To meet the challenges and the requirements of the industries, the interest in developing high strength Al-based amorphous alloys have been increased.

The strength of light weight Al-based alloys could be enhanced from about 600 MPa in the age hardened condition to over 1500 MPa in the amorphous-based alloys or nanocomposites [2]. Al-based amorphous materials can be produced through several methods, namely, mechanical alloying (MA), rapid solidification processing (RSP), physical and chemical vapor depositions, sputter deposition and gas atomization. Out of these, MA and RSP are known to generate metastable structures by non-equilibrium techniques. These methods have been extensively employed to generate Al-based amorphous alloys [3, 4].

In the MA process powder blends of desired nominal compositions are subjected to high energy ball milling to promote alloying at atomic scale at near-ambient temperature, and it is used to develop metastable microstructures, like amorphous structures, in the powder product. On the other hand, RSP by melt spinning is a process of converting a liquid material into a solid by quick removal of heat. In the RSP a rotating copper wheel is cooled internally usually by water or liquid nitrogen. A thin stream of molten liquid is dripped onto the rotating wheel causing its rapid solidification at a high cooling rate, of the order of 10^4–10^7 K/s [5].

Al-based glasses are generally produced by rapid quenching, such as melt spinning [6, 7] or by mechanical alloying [4] however, these processes limit the size of the glassy samples to the shape of thin ribbons or in the form of fine powders. Therefore, further consolidation is required to produce amorphous based bulk samples to evaluate their mechanical properties [8-10] from RSP products or mechanically alloyed powder products.

The amorphous phase formed during RSP of Al−Si−Ni alloys has already been reported in literature [11]. An amorphous phase was formed over wide composition range from about 14 to 25 % Si and 8 to 25 % Ni.

Therefore, in the present study, seven such alloys, namely, $Al_{75}Si_{15}Ni_{10,}$ $Al_{70}Si_{20}Ni_{10,}$ $Al_{65}Si_{25}Ni_{10}$, $Al_{70}Si_{15}Ni_{15}$, $Al_{65}Si_{20}Ni_{15}$, $Al_{78}Si_{14}Ni_{8}$ and $Al_{50}Si_{25}Ni_{25}$ were designed for high energy ball milling up to 50 h to evaluate the phase formation characteristics by MA of these compositions. The phase evolution characteristics of these alloys by the two non-equilibrium methods could provide important information. The microstructural and thermal properties of these alloys have been investigated by X- ray diffraction (XRD), Scanning electron microscopy (SEM), Transmission electron microscopy (TEM), Fourier transform infrared spectroscopy (FTIR), Nano zeta sizer (NZS), Differential scanning calorimetry (DSC). Finally, the structures and properties are correlated.

1.2 Aim and Scope of Present Study

The present study explores the effectiveness of MA for synthesizing the Al-based Al-Si-Ni alloys and the aim of the present study can be enumerated as follows:

a) MA of seven Al-rich compositions, namely, $Al_{75}Si_{15}Ni_{10,}$ $Al_{70}Si_{20}Ni_{10,}$ $Al_{65}Si_{25}Ni_{10}$, $Al_{70}Si_{15}Ni_{15}$, $Al_{65}Si_{20}Ni_{15}$, $Al_{78}Si_{14}Ni_{8}$ and $Al_{50}Si_{25}Ni_{25}$.
b) Study the phase evolution of these alloys by XRD.
c) Study the microstructural details by SEM and EDX analysis.

d) Characterize the particle size and crystalline nature of the 50 h milled samples by TEM.

e) Study the percentage transmittance of the milled product by FTIR to correlate with reduction in particle size during milling.

f) Analysis of the particle size distribution by Nano Zeta Sizer using the percentage transmittance.

g) Evaluate the thermal property of the final products by DSC.

h) Analysis of the XRD data to investigate the possible reason for the amorphous phase formation by MA.

i) To compare their structures generated by MA with those reported for RSP of the same composition.

j) To investigate the possible reasons for the divergence of the structures generated by MA compared to that of RSP.

CHAPTER 2 Literature Review

2.1 Al-based amorphous alloys

2.1.1 Rapid solidification processing (RSP)

Since the first synthesis of an amorphous phase in an Au-Si system by rapid solidification in 1960 [12], a great number of amorphous alloys have been synthesized by various preparation methods of rapid quenching from liquid or vapor and solid-state reactions [13, 14]. However, the maximum thicknesses of the resulting amorphous alloys have normally been limited to less than 100 μm. The restriction of the maximum sample thickness has prevented a broad extension of application fields of amorphous alloys. Accordingly, great efforts have been devoted to synthesis of a bulk amorphous alloy from amorphous alloy powder by using various experimental techniques of warm pressing, warm extrusion, explosive compaction etc. [15]. Still, there have been no successful data on the production of a bulk amorphous alloy having the same mechanical, chemical and soft magnetic properties as those for the corresponding melt-spun amorphous alloy ribbons. Due to the poor engineering properties of the consolidated bulk amorphous alloys, the bulk amorphous alloys had not gained any practical applications. Under such a critical situation, amorphous alloys with much higher glass-forming ability have been found in a number of alloy systems such as Mg-Ln-TM [16], Ln-Al-TM [17], Zr-Al-TM [18], Ti-Zr-TM [19], Zr-Ti-TM-Be [20] Zr-(Ti, Nb, Pd)-Al-TM [21], Pd-Cu-Ni-P [22], Fe-(Al, Ga)-(P, C, B, Si)[23], (Fe, Co, Ni)-(Zr, Hf, Nb)-B [24] and Pd-Ni-Fe-P[25] (Ln=lanthanide metal, TM=transition metal). The use of the new multicomponent alloy systems has enabled the production of bulk amorphous alloys within a thickness range up to about 75 mm by conventional solidification methods [26]. These bulk amorphous alloys exhibit the same mechanical and magnetic properties as those for the corresponding melt-spun amorphous alloy ribbons and have been expected to be used as new engineering materials.

2.1.1.1 Binary alloy system

The formation of Al-based amorphous alloys by liquid quenching was first tried in binary alloys of Al-metalloid and Al-transition metal (M) systems. It was found in Al-Si [27], Al-Ge [28] and Al-M (M=Cu [29], Ni [30], Cr [31] or Pd [32] alloys that a coexistent structure of amorphous and crystalline phase is formed only near the holes in their thin foils prepared by the gun quenching technique in which the cooling rate is higher than that for the melt spinning method. However, no amorphous phase without crystallinity was prepared by melt spinning as well as by the gun- and piston-anvil methods.

2.1.1.1.1 Al-rare earth metal (Al-R) amorphous alloys

Amorphous alloys was found in Al-R (R=Y, La, Ce, Pr, Nd, Sm, Gd, Tb, Dy, Ho, Er or Yb) binary systems. The amorphous phase is formed in the compositional ranges 9-13% Y, 7-11% La or Ce, 10% Pr, 8-12% Nd or Gd, 8-6% Sm, 9-14% Tb and 9-12% of Dy, Ho, Er or Yb. Thus, the glass formation range is the widest for Al-Sm, followed by Al-Tb, Al-(Y, Nb or Gd), Al-(La, Ce, Dy, Ho, Er or Yb) and then Al-Pr [33, 34].

2.1.1.2 Ternary alloy system

The first formation of an amorphous single phase in Al-based alloys containing more than 50 at% Al was found in 1981 for Al-Fe-B and Al-Co-B ternary alloys [35]. However, these amorphous alloys are highly brittle and hence have not attracted much attention. Afterwards, an amorphous phase was found in melt-spun Al-Fe-Si, Al-Fe-Ge and Al-Mn-Si alloys [36] but they were also brittle, similar to the Al-(Fe or Co)-B amorphous alloys. It was observed from these data that the brittleness might be an integral property for Al-based amorphous alloys. However, in 1987, an amorphous phase with good bending ductility was discovered by Inoue et al. [11] to be formed at compositions above about 80 at% Al in Al-Ni-Si and Al-Ni-Ge systems. Since the discovery, ductile Al-based amorphous alloys have successively been observed in a number of ternary alloys consisting of Al-early transition metal (EM)-late transition metal (LM) [37], which are illustrated by Al-Zr-Cu, Al-Zr-Ni and Al-Nb-Ni. Here, EM

is the IV-VI group transition metals and LM is VII and VIII group transition metals. These were followed by Al-rare earth metal(R) LM ternary alloys [38] in which the EM is substituted by R. Al-based amorphous with higher glass-forming ability and better mechanical strength have been obtained in ternary alloys without metalloid elements like Al-EM-LM and Al-R-LM.

2.1.1.2.1 Al-EM-LM amorphous alloys

The effect of EM (EM=Ti, Zr, Hf, V, Nb, Ta, Cr, Mo or W) elements on the glass formation of $Al_{70}Fe_{20}M_{10}$, $Al_{70}Co_{20}M_{10}$ and $Al_{70}Cu_{20}M_{10}$ alloys by melt spinning was studied by Tsai et al.[37, 39] The effectiveness of the M elements to form an amorphous phase was the greatest for Zr and Hf and decreases in the order of Ti>V>Mo>Nb>Cr>Ta. No amorphous phase was observed in the Al-based alloys containing W. Thus, alloys composed of the LM of Fe, Co, Ni and Cu, and the EM of Ti, Zr, Hf etc., and Al can form metal-metal type Al-based amorphous structures. It was also notable that the formation of the amorphous alloys extends over rather wide compositional ranges around the Al_7 $(LM)_2(EM)_1$ compositions.

The reason for the glass formation of the metal-metal type Al-based alloys was briefly discussed. The amorphous alloys are composed of Al, LM and EM. Furthermore, most of the binary alloys consisting of LM and EM except Al can be amorphized by melt spinning as illustrated for Fe-(Zr or Hf), Co-(Ti, Zr or Hf), Ni-(Ti, Zr or Hf) and Cu-(Zr or Hf) [40]. It has usually been known that the amorphization of alloys is closely related to the ratio of glass transition temperature (T_g) to melting temperature (T_m), i.e. the reduced glass transition temperature (T_g/T_m), and the larger the reduced glass transition temperature the higher the glass-forming tendency. Although the T_m of Al-Cu alloys decreases with increasing Cu content in the range below 17.3%, T_m of the other Al-M binary alloys rises rapidly with increasing M content [41]. However, due to the presence of the LM and EM, the rise of T_m of the Al-based ternary alloys is thought to be significantly decreased because many eutectic points exist in the binary alloys of LM and EM [41]. A set of intermetallic compounds was observed in Al-M alloys as well as in EM-LM alloys. It was therefore assumed that the attractive interaction among the constituent elements is significantly raised by adding the EM to the Al-LM binary

alloys, leading to the increase in the viscosity of supercooled liquid and its temperature dependence, which causes the enhancement of glass formation. The decrease of T_m and the increase of the attractive interaction among the constituent elements by the coexistence of Al, LM and EM seem to be dominant factors for the amorphization of the present metal-metal type amorphous alloys.

2.1.1.2.2 Al-rare earth metal (R)-transition metal (M) amorphous alloys

Amorphous phase was found in Al-Y-M, Al-La- M and Al-Ce-M (M=Fe, Co, Ni or Cu) alloy systems by melt spinning. The formation ranges of Al-Y-M and Al-Ce-M amorphous alloys were the widest for the Al-Y-Ni and Al-Ce-Ni systems. No distinct difference was seen among the other three alloys in the Al-Y-M and Al-Ce-M systems, while those for the Al- La-M amorphous alloys were the narrowest for the Al-La-Cu system and much wider for the other Al-La-(Fe, Co, Ni) systems. Accordingly, the effectiveness of M elements on the compositional range for formation of the Al-based amorphous alloys was the largest for Ni, followed by Fe, Co and then Cu. These amorphous alloys containing more than about 80% Al can be completely bent by 180^0 without fracture, and no considerable crack was observed even in the severely deformed area. The ductility of the Al-R-M amorphous alloys was strongly dependent on alloy composition and there was a clear tendency for the ductility to increase with increasing Al content.

2.1.2 Al-based bulk amorphous alloys

There are various methods of producing Al-based bulk amorphous alloys. Among these three most significant methods are mold casting, high-pressure die casting and warm extrusion.

2.1.2.1 Metallic mold casting

In production of bulk amorphous alloys by the metallic mold casting method, it has been reported [42] that the maximum sample thickness (t_m) is proportional to the temperature interval of the supercooled liquid region which is defined by the difference

between T_g and ΔT_x, $\Delta T_x(=T_x-T_g)$. Al- based amorphous alloys with high strength and good ductility has ΔT_x values of about 20-30 K. The relation between ΔT_x and T_m leads us to expect that bulk amorphous alloys are also produced in Al-based alloys by the metallic mold casting method.

Ternary alloys with alloy compositions of $Al_{84}Ni_8Y_8$, $Al_{84}Ni_{10}La_6$ and $Al_{84}Ni_{10}Ce_6$ were chosen because they had the largest ΔT_x in each alloy system and were expected to have the highest glass-forming ability. In addition to the three alloys, ternary $Al_{100-x-y}Ni_xCe_y$ alloys were also used for the examination of the influence of the supercooled liquid region on the production of an amorphous sheet. Thick sheet samples with a constant width of 5 mm and thicknesses of 0.1-0.5 mm were prepared by injection casting of the melt into copper molds with inner shapes of rectangular parallelepiped. It is thus concluded that the metallic mold casting causes the formation of an amorphous phase which is similar to that for the ribbon sample obtained by melt spinning. In addition, the critical sheet thickness for formation of an amorphous phase appears to lie in the range of 0.3-0.4 mm in the present metallic mold casting condition.

2.1.2.2 High-pressure die casting

As one method of producing bulk amorphous alloys with high σ_f, one can list a high-pressure die casting method which enables a simultaneous accomplishment of high cooling rate and direct production into various final shapes. $Al_{84}Ni_{10}Ce_6$ amorphous phase in sheet and cylinder shapes with much larger thicknesses was developed by high-pressure die casting [43].

2.1.2.3 Warm extrusion of atomized powder

The production of Al -Ni-Y amorphous powders was tried by high-pressure helium atomization. The size fraction of the amorphous Al-Y-Ni powder was measured by the microtrac analysis method. The fraction is 41% for the powder below 10 μm in size, followed by 24% for the powder between 10 and 15 μm in size, 25% for the 15-21 μm powder and 11% for the powder above 21 μm in size. It was thus significant that the powder below 15 μm in size was prepared with a high yield fraction of 65%.Furthermore, the DSC curve obtained from the $Al_{85}Y_{10}Ni_5$ amorphous powder was confirmed to be the same as that for the melt-spun amorphous ribbon, and no

appreciable difference in T_g and T_x was seen by Inoue et al. [44]. It is therefore concluded that the amorphous powder produced by high-pressure helium atomization can be used as a raw material to produce an amorphous bulk by consolidation at temperatures near T_g.

2.1.3 Mechanical alloying

Mechanical alloying (MA) is a solid-state powder processing technique involving repeated cold welding, fracturing, and rewelding of powder particles in a high-energy ball mill. Earlier, the method of MA was developed in the 1970's for the production of thoria dispersed nickel (TD Nickel) based superalloys. MA has now the capability of synthesizing a variety of metastable phases starting from elemental powder blends to pre-alloyed powders with ductile-ductile or ductile-brittle or brittle-brittle combinations of materials.

2.1.3.1 Process Variables

Mechanical alloying is a complex process and hence involves optimization of a number of variables to achieve the desired product phase and/or microstructure. Some of the important parameters that have an effect on the final constitution of the powder are:

- Type of mill
- Milling container
- Milling speed
- Milling time
- Type, size, and size distribution of the grinding medium
- Ball-to-powder weight ratio
- Extent of filling the vial
- Milling atmosphere
- Process control agent
- Temperature of milling

All these process variables are not completely independent. For example, the optimum milling time depends on the type of mill, size of the grinding medium, temperature of milling, ball-to-powder ratio, etc.

2.1.3.1.1 Type of mill

There are a number of different types of mills for conducting MA. These mills differ in their capacity, speed of operation, and their ability to control the operation by varying the temperature of milling and the extent of minimizing the contamination of the powders. Depending on the type of powder, the quantity of the powder, and the final constitution required, a suitable mill can be chosen. Most commonly, however, the SPEX shaker mills are used for alloy screening purposes. The Fritsch Pulverisette planetary ball mills or the attritors are used to produce large quantities of the milled powder. Specially designed mills are used for specific applications.

2.1.3.1.2 Milling container

The material used for the milling container (grinding vessel, vial, jar, or bowl are some of the other terms used) is important since due to impact of the grinding medium on the inner walls of the container, some material will be dislodged and get incorporated into the powder. This can contaminate the powder or alter the chemistry of the powder. If the material of the grinding vessel is different from that of the powder, then the powder may be contaminated with the grinding vessel material. On the other hand, if the two materials are the same, then the chemistry may be altered unless proper precautions are taken to compensate for the additional amount of the element incorporated into the powder. Hardened steel, tool steel, hardened chromium steel, tempered steel, stainless steel, WC-Co, WC- lined steel [45] and bearing steel are the most common types of materials used for the grinding vessels [46].

2.1.3.1.3 Milling speed

The faster the mill rotates the higher would be the energy input into the powder. But, depending on the design of the mill there are certain limitations to the maximum speed

that could be employed. For example, in a conventional ball mill increasing the speed of rotation will increase the speed with which the balls move. Above a critical speed, the balls will be pinned to the inner walls of the vial and do not fall down to exert any impact force. Therefore, the maximum speed should be just below this critical value so that the balls fall down from the maximum height to produce the maximum collision energy. Another limitation to the maximum speed is that at high speeds (or intensity of milling), the temperature of the vial may reach a high value. This may be advantageous in some cases where diffusion is required to promote homogenization and/or alloying in the powders. But, in some cases, this increase in temperature may be a disadvantage because the increased temperature accelerates the transformation process and results in the decomposition of supersaturated solid solutions or other metastable phases formed during milling [47]. Milling speed of 300 rpm was set during MA of this present composition.

2.1.3.1.4 Milling time

The time of milling is the most important parameter. Normally the time is so chosen as to achieve a steady state between the fracturing and cold welding of the powder particles. The times required vary depending on the type of mill used, the intensity of milling, the ball-to-powder ratio, and the temperature of milling. These times have to be decided for each combination of the above parameters and for the particular powder system. But, it should be realized that the level of contamination increases and some undesirable phases form if the powder is milled for times longer than required [48]. Therefore, it is desirable that the powder is milled just for the required duration and not any longer. Milling time of 50 h was chosen for this work.

2.1.3.1.5 Grinding medium

Hardened steel, tool steel, hardened chromium steel, tempered steel, stainless steel, WC-Co, and bearing steel are the most common types of materials used for the grinding medium. The density of the grinding medium should be high enough so that the balls create enough impact force on the powder. It is always desirable to have the grinding vessel and the grinding medium made of the same material as the powder

being milled to avoid cross contamination. Stainless steel was used as grinding medium for present study during MA.

The size of the grinding medium also has an influence on the milling efficiency. A large size (and high density) of the grinding medium is useful since the larger weight of the balls will transfer more impact energy to the powder particles. It has also been reported that the final constitution of the powder is dependent upon the size of the grinding medium used. For example, when balls of 15 mm diameter were used to mill the blended elemental Ti-Al powder mixture, a solid solution of aluminum in titanium was formed. On the other hand, use of 20 and 25 mm diameter balls resulted in a mixture of only the titanium and aluminum phases, even after a long milling duration [48].

It was suggested that the smaller balls produced intense frictional action, which promoted the amorphous phase formation. In fact, it appears that ``soft" milling conditions (small ball sizes, lower energies, and lower ball-to-powder ratios) seem to favor amorphization or metastable phase formation [49]. It has been predicted that the highest collision energy can be obtained if balls with different diameters are used. It has been reported that a combination of large and small size balls during milling minimizes the amount of cold welding and the amount of powder coated onto the surface of the balls.

2.1.3.1.6 Ball-to-powder weight ratio (BPR)

The ratio of the weight of the balls to the powder (BPR), sometimes referred to as charge ratio (CR), is an important variable in the milling process. This has been varied by different investigators from a value as low as 1:1 to as high as 220:1.Generally speaking, a ratio of 10:1 is most commonly used while milling the powder in a small capacity mill such as a SPEX mill. But, when milling is conducted in a large capacity mill, like an attritor, a higher BPR of up to 50:1 or even 100:1 is used. The ball to powder weight ratio of 10:1 was taken for present study.

The higher the BPR, the shorter is the time required. For example, formation of an amorphous phase was achieved in a Ti- 33at%Al powder mixture milled in a SPEX mill in 7 h at a BPR of 10:1, in 2 h at a BPR of 50:1 and in 1 h at a BPR of 100:1 [50]. At a high BPR, because of an increase in the weight proportion of the balls, the number of collisions per unit time increases and more energy is transferred to the powder particles consequently alloying takes place faster

2.1.3.1.7 Extent of filling the vial

Since alloying among the powder particles occurs due to the impact forces exerted on them, it is necessary that there is enough space for the balls and the powder particles to move around freely in the milling container. Therefore, the extent of filling the vial with the powder and the balls is important. If the quantity of the balls and the powder is very small, then the production rate is very small. On the other hand, if the quantity is large, then there is not enough space for the balls to move around and so the energy of the impact is less. Thus, care has to be taken not to overfill the vial; generally about 50% of the vial space is left empty.

2.1.3.1.8 Milling atmosphere

Different atmospheres have been used during milling for specific purposes. Nitrogen or ammonia atmospheres have been used to produce nitrides. Hydrogen atmosphere was used to produce hydrides. The presence of air in the vial has been shown to produce oxides and nitrides in the powder, especially if the powders are reactive in nature. Thus, care has to be taken to use an inert atmosphere during milling [51].

2.1.3.1.9 Process control agents

A process control agent (PCA) is added to the powder mixture during milling to reduce the effect of cold welding. The nature and quantity of the PCA used and the type of powder milled would determine the final size, shape, and purity of the powder particles. Use of a larger quantity of the PCA normally reduces the particle size by 2-3 orders of magnitude. For example, Lu and Lai [48] have reported that milling of aluminum for 5 h produced a particle size of about 500 mm when 1 wt% stearic acid was used as a

PCA. But, when 3 wt% of stearic acid was used; the particle size was only about 10 mm. The amount of the PCA is dependent upon the (a) cold welding characteristics of the powder particles, (b) chemical and thermal stability of the PCA, and (c) amount of the powder and grinding medium used. The most important of the PCAs include stearic acid, hexane, Toluene, methanol, and ethanol. Toluene was used as a process control agent for present investigation.

2.1.3.1.10 Temperature of milling

There have been conflicting reports on the formation of an amorphous phase as a function of the temperature of milling. Amorphization during MA involves formation of micro-diffusion couples of the constituent powders followed by a solid-state amorphization reaction. Thus, higher milling temperatures should enhance the amorphization kinetics. This has been observed in the Ni-Zr [52] systems. During milling of a Ni-50at%Zr powder mixture in a vibrating mill, amorphous phase formation was not observed when the powder was milled at liquid nitrogen temperature for 15 h. On the other hand, milling for the same period of time produced a fully amorphous phase at 200ºC; a partially amorphous phase was produced on milling at room temperature. Lower milling temperatures are expected to favor amorphization. However, both increased and decreased kinetics have been reported. Milling was carried out in room temperature for present study.

2.1.3.2 Mechanism of alloying

During milling when two hard balls collide, a very small amount of powder is entrapped in between them. Typically, around 1000 particles are trapped during each collision (Fig. 2.1). The impact force deforms the powder particles plastically leading to work hardening and fracture. The new surfaces created enable the particles to weld together and this leads to an increase in particle size in case of ductile-ductile or ductile-brittle combination of materials. At this stage, the composite particles have a characteristic layered structure (Fig. 2.3) consisting of various combinations of the starting constituents. With continued deformation, the particles get work hardened and

fractured/fragmented of fragile flakes. At this stage, the tendency to fracture dominates over cold welding. Due to the continued impact of grinding balls, the structure of the particles gets steadily refined, but the particle size continues to be the same after certain duration of milling. Steady-state equilibrium is reached when a balance is achieved between the rate of cold welding and the rate of fracturing. At this stage each particle contains substantially all of the starting ingredients in the same proportion of initial composition.

During MA, a variety of crystal defects such as dislocations, vacancies, stacking faults, and increased number of grain boundaries are introduced. The defects such as dislocations, vacancies, stacking faults etc., which are introduced during MA, enhance the diffusivity of solute elements into the matrix. The diffusion distance is also reduced due to refinement of the microstructure. Moreover, the slight rise in temperature of the material during milling also aids the diffusion. Consequently, true alloying takes place amongst the constituent elements [4].

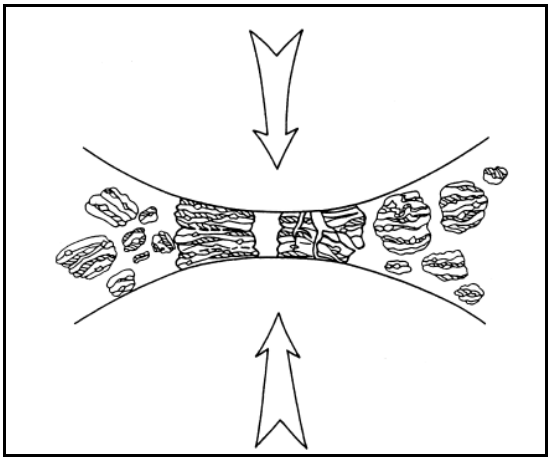

Fig 2.1: Ball-powder-Ball collision of powder mixture during MA

In planetary ball mill the centrifugal force produced by the vials rotating around their own axes and that produced by the rotating support disk both act on the vial contents, consisting of material to be ground and the grinding balls. Since the vials and the supporting disk rotate in opposite directions, the centrifugal forces alternately act in

like and opposite directions. This causes the grinding balls to run down the inside wall of the vial- the friction effect, followed by the material being ground and grinding balls lifting off and traveling freely through the inner chamber of the vial and colliding against the opposing inside wall -the impact effect (Fig. 2.2).

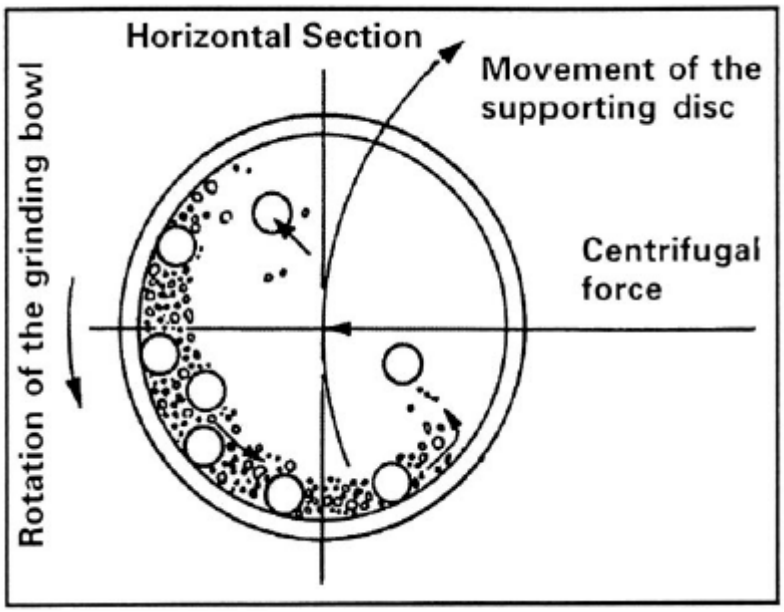

Fig. 2.2: Schematic diagram depicting the ball motion inside the ball mill

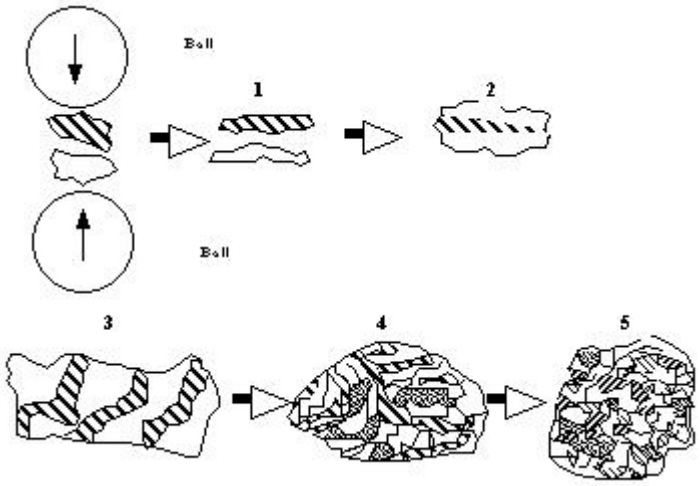

Fig 2.3: Layered structured formed during mechanical alloying.

2.1.3.3 Advantages of Mechanical Alloying

MA is a simple and an economically feasible process with important technical advantages.

- Usually, we make alloys by melting together the components, whereas, Mechanical alloying involves the synthesis of materials in solid state by high-energy ball milling.
- Bulk material with dimension larger than rapid solidification process (RSP) can be produced by MA.
- Synthesis of novel alloys, e.g., alloying of normally immiscible elements, which is not possible by any other technique like RSP. This is because MA is a completely solid state processing technique and therefore limitations imposed by phase diagrams don't apply here.
- Extended solid solubility was achieved by MA in some alloy system. This technique can be used to induce chemical displacement reactions in powder mixtures at room temperature or at much lower temperature than normally required to synthesize pure metals .

- MA can be used for the refinement of the matrix microstructure down to nanometer range. These nanostructures obtained not by clustered assembly but by the structural decomposition of coarser grained structures as the result of severe plastic deformation [53]

- Amorphous phase formation is one of the most frequently reported phenomena in mechanically alloyed powder mixtures.

2.1.3.4 Amorphization in binary alloy system

Mechanical Alloying (MA) was first developed by John Benjamin et al. [54] at International Nickel in the late 1960's in order to produce oxide-dispersion-strengthened (ODS) alloys for high temperature structural applications. Since that time

there have been many studies using the MA of dissimilar powder and mechanical milling (MM) of single composition powders (such as intermetallic compounds) to synthesize nonequilibrium structures: microstructures including amorphous alloys, extended solid solutions, metastable crystalline phases, quasicrystals and nanocrystalline materials. The first suggestion that MA might produce amorphous material was made by White [55] during a study of the synthesis of superconducting Nb_3Sn via MA and subsequent thermo mechanical treatment. The first definitive study of amorphization by MA was carried out by Koch et al. [56] in the easy-glass-forming alloy system Ni-Nb. The diffraction pattern for MA $Ni_{60}Nb_{40}$ powder for milling times greater than 10 h exhibits an amorphous type pattern comparable to that for amorphous $Ni_{60}Nb_{40}$ which was rapidly solidified.

The synthesis of amorphous structure in binary alloy system was reported by many authors. Followings are progress of development of some Al-based amorphous alloys.

Koyabashi [57] reported the amorphous phase formation in binary alloy system of Al-Cr. Al-15at%Cr and Al-24at%Cr alloys were MA by ball milling to yield composite metal powders and homogeneously alloyed powders. On heating the 15% alloy, which has been milled for 800 and 1000 hours, exothermic reactions were detected at two temperatures. On quenching the material form just above the lower of these temperatures, X-ray diffraction and transmission electron microscopy showed it to be amorphous.

S. Abe [58] observed the amorphous phase formation in binary alloy system of Al-Ti.MA was used produce amorphous alloy from Al-20%Ti powder mixture in a attritator ball mill. During MA flake formation, cold welding and fracturing of particles formation of solid solution and amorphization were detected by optical and electron microscopy, X-ray analysis and hardness measurement. After MA of 137 hours, the amount of 17% Ti was found dispersed from lattice parameter measurement. The grain size in the particles was 20-60 nm. After MA of 600 hours the powder was amorphous with a mean particle size of 600 nm. The observed increase in hardness was attributed to solid solution, work hardening and dispersion of Al_2O_3.

Huang et al. [59] reported the formation of amorphous phase in Al-Fe alloy system by MA. It was found that the formation of amorphous phase and extended solid solution of Fe in fcc Al takes place in Al rich alloys, and almost entirely amorphous structures appears for composition from 17 to 33at%Fe.

Dong [60] reported the formation of amorphous phase in Al-Fe binary system. crystalline elemental powders of Al_xFe_{100-x} (x=40-90) were mechanical alloyed by high energy ball mill. The TEM study showed that the structure of alloy containing (50-80) at. % Al is basically amorphous, while the alloys out of this range are of nanocrystalline phase. A further investigation by high resolution TEM showed that very few nanometer order crystallites still existed in the amorphous matrix of the $Al_{80}Fe_{20}$ alloy. It was suggested that 100% amorphization cannot be achieved in Al-Fe binary system in practice by mechanical alloying.

Sherif El-Eskandarany et al. [61] reported the effect of the ball-to-powder weight ratio on the amorphization reaction of $A1_{50}Ta_{50}$ alloy powders using the ball milling technique. As the ball-to-powder weight ratio increases, the rate of amorphization reaction increases drastically, but the content of iron contamination, which comes from the milling tools, increases sharply. A complete amorphous phase was obtained with a ball-to-powder ratio in the range between 36: 1 and 108: 1 under those experimental conditions

Cardellini et al. [62] reported the solid state reactions and the microstructural evolution during high-energy ball milling of Al-Ni powder mixtures in the composition range 25-75 at.% Al. microscopic mechanism underlying the alloying process in this system is the diffusion of Ni atoms in the Al-rich layers and that an important role is played by the oxygen contamination. An amorphous Al-rich phase containing a few at.% oxygen and with a Ni content not exceeding approximately 50 at.% was detected in the equiatomic and Ni-rich samples milled for a few hours.

K. Chattopadhyay et al.[63] reported the mechanical alloying behavior of elemental aluminium with diamond cubic elements Ge and Si. A metastable crystalline phase with rhombohedral crystal structure was observed in $Al_{70}Ge_{30}$ and $Al_{60}Ge_{40}$ alloy

compositions. No such metastable phase was observed in the Al-Si system. They also reported X-ray diffractometry and differential scanning calorimetry results suggestive of amorphization

It is known that amorphous alloys of metal-carbon systems are difficult to manufacture by mechanical alloying of the elemental powder mixture. Ball milling of M-C (M=Ni,Co) mixtures blend has resulted in supersaturated solid state solution or metastable phase M_3C instead of in a amorphous phase. However, Wu et al. [64] reported amorphous phase formation during MA of elemental Al and graphite. The Al-C system has advantages in comparison to other (M-C) binary alloy system. The Al-Al_4C_3 composite fabricated by MA has special advantage of good mechanical properties retain at elevated temperature in addition to excellent room temperature properties.

The crystallization process of amorphous $Al_{80}Fe_{20}$ alloy powders prepared by ball milling was investigated by Zhou et al. [65]. The amorphous-to-crystalline transition during thermal annealing of amorphous $Al_{80}Fe_{20}$ alloy powders was observed by means of magnetothermal analysis and X-ray diffraction. A metastable phase precipitated during primary crystallization, and a mixture of intermetallic compound ($_{\theta}$-$Al_{13}Fe_4$) and fcc Al was developed further.

Gu et al. [66] reported the pressure effect on the crystallization of amorphous $Al_{85}Fe_{15}$ alloy prepared by means of ball-milling in the year 1999. Alloy was investigated in a pressure range up to 1.4 GPa. It was found that the applied pressure enhances the nanoscale fcc Al precipitation from amorphous matrix which does not occur at ambient pressure. The precipitation temperature of nanoscale fcc Al from amorphous matrix decreases from about 380 to 200°C when the applied pressure increases from 0.4 to 1.0 GPa. The high-pressure annealing of mechanically alloyed Al-based amorphous powders provides an effective approach to optimize the synthesis procedure for nanocrystalline/amorphous composite materials.

Aluminum based composite materials reinforced by various high-temperature resistant ceramic fine particulates, such as SiO2, SiC, Si3N4, TiC and other powders, have been synthesized by MA procedure, displaying a desirable enhance of mechanical properties at room and elevated temperatures. Wang et al. [67] reported that ball milling of the mixtures of SiO_2 and Al powders results in an amorphous phase after milling for 150 h. It was found that the atmospheres during milling have a greatly impact on the final product. Amorphization was observed in the MA process under argon atmosphere, while MA under air atmosphere the starting materials were still present. It was believed that the amorphization is due to the destabilization of crystalline phase, induced by refinement of grain size, vitrification of pressure, and loss of long range of order in supersaturated solid solution due to interdiffusion.

2.1.3.5 Amorphization in multicomponent alloy system

The amorphization in multicomponent Al-based alloy was investigated by many authors in recent years. These are list of some Al-based amorphous alloy developed by various researchers.

Wilson et al. [68] reported Amorphization and crystallization processes of the ball-milled Al–Y–Fe–TM alloys (TM = Ni, Co, Cu, and Fe) in 2006. High-energy ball milling was used to synthesize aluminum-based alloys containing amorphous and nanocrystalline phases to investigate the compositional effects of transition metals (TM) on the amorphization and crystallization processes of the ball-milled $Al_{85}Y_7Fe_5TM_3$ alloys (TM = Ni, Co, Cu, and Fe) were investigated. The crystallization kinetics of the ball-milled Al–Y–Fe–TM nanocomposite powders were studied using differential scanning calorimetry (DSC). The DSC results of $Al_{83}Y_7Fe_5Ni_5$ showed that the crystallization temperature and the activation energy of crystallization were 668 K and 310 kJ/mol, respectively. In-situ high-temperature X-ray diffraction was carried out which showed that the crystallization was a complex process involving growth of the nanocrystalline phase along with crystallization of the amorphous matrix phase.. When one TM component is substituted with another TM component of similar atomic size, the intensity of the crystalline peaks in the XRD patterns changed as the enthalpy of mixing, ΔH_{mix}, for Al and TM changed. The general trend was observed that the alloys

with the highest eutectic temperature of the binary alloy (Al–TM) also had the highest onset of crystallization temperature.

The compositional effect on amorphous phase formation was studied by Samanta et al. [69] in the year 2007. Mechanical alloying of Al-rich Al–Ni–ETM (ETM = Ti, Nb, Zr) elemental powder blends by planetary ball milling yielded amorphous and/or nanocrystalline products after ball milling for suitable duration. Powder samples collected at different stages of ball milling was examined by X-ray diffraction, differential scanning calorimetry and high-resolution transmission electron microscopy to examine the solid-state phase evolution. Powder blends having nominal composition of $Al_{80}Ni_{10}Ti_{10}$ and $Al_{80}Ni_{10}Nb_{10}$ yielded predominantly amorphous products, whereas, the other alloys formed composite microstructures comprising nanocrystalline and amorphous solid solutions. In the case of $Al_{65}Ni_{20}Ti_{15}$ powder blend after initiation of amorphization, formation of thermodynamically stable AlNi phase hindered the further progress of amorphization of the powder blend. Similar evidence of incomplete amorphization was observed in $Al_{65}Ni_{20}Zr_{15}$ and $Al_{65}Ni_{20}Nb_{15}$ powder blends due to the formation of AlNi phase at some intermediate stages of ball milling.

Manna et al. [70] reported the compositional effect on amorphization in Al-Cu-Zr system in 2004. Mechanical alloying was carried out in $Al_{65}Cu_{35-x}Zr_x$ (x=5, 15 and 25 at.% Zr) elemental powder blends by planetary ball milling up to 50 h. The phase evolution of the milled product at different stage of milling was during milling was characterized by X-ray diffraction, (XRD) high-resolution transmission electron microscopy (TEM) and energy dispersive X-ray spectroscopy (EDS). Among the different alloys synthesized by mechanical alloying, $Al_{65}Cu_{20}Zr_{15}$ yields a predominantly amorphous product, whereas, the other two alloys develop a composite microstructure comprising nanocrystalline and amorphous solid solutions in $Al_{65}Cu_{10}Zr_{25}$ and nano-intermetallic phase/compound in $Al_{65}Cu_{30}Zr_5$, respectively. So from present investigation by the author it can be concluded that composition of alloying element plays an important role in amorphous phase formation of the final product.

Chen et al. [71] reported effect of composition on amorphous phase formation. Ce-substitution for Al in the $Al_{90-x}Fe_5Ni_5Ce_x$ (x = 0, 2, 5, 7, 8, 9, and 10) system on the mechanical alloying process were investigated. The microstructural evolution in these powders was characterized by scanning electron microscopy, differential thermal analysis and X-ray diffraction techniques. The compositional range of amorphous phase forming was obtained and it extended from 5 to 9 at. % Ce. With increasing Ce content, the crystallization temperature of amorphous alloys The compositional range of amorphous forming was obtained and it extended from 5 to 9 at.% Ce. With increasing Ce content, the increase of crystallization temperature of amorphous alloys was observed.

Zhang et al. [72] reported the effect of prolonged milling on the amorphous phase formation. A ternary elemental powder mixture with a composition of Al–27.4at%Fe–28.7at%C was milled by using a high energy ball mill. Phase formation during high energy ball milling and during low temperature heat treatment of the milled powder was studied. It was found that an amorphous phase formed during prolonged milling. Mechanical alloying of Al, Fe and C elemental phases enables formation of an amorphous phase, while low temperature heat treatment of mechanically milled powder facilitates formation of AlFe and $AlFe_3$ $C_{0.5}$ phases.

Mula et al. [73] reported wide difference in the atomic size of the alloying elements in solid solution plays an important role in the amorphous phase formation. An elemental blend of $Al_{94.5}Cr_3Co_{1.5}Ce_1$ was mechanical alloyed in a high energy ball mill. Amorphous and nanocrystalline phases generated during milling were studied by X-ray diffraction (XRD), transmission electron microscopy (TEM), scanning electron microscopy (SEM) and differential scanning calorimeter (DSC). MA of $Al_{94.5}Cr_3Co_{1.5}Ce_1$ composition carried out in the present study showed the formation of Al-based solid solutions along with partial amorphization. A wide variation in the lattice parameter of the Al-rich solid solution caused by some suitable combination of the alloying additions (*e.g.* Cr, Co and Ce) played an important role in the amorphization during MA.

Singh et al. [9] reported laser sintering on mechanically alloyed $Al_{50}Ti_{40}Si_{10}$ powders with partially amorphous and nanocrystalline microstructure in 2009. Microstructure and mechanical properties on top surface and cross-sectional plane were evaluated by scanning and transmission electron microscopy, X-ray diffraction, hardness measurement and fretting wear testing. Very high hardness (745.2H*v*), excellent wear resistance (2.02×10^3 μm^3) and homogeneous microstructure without macro-defects or cracks from the sintered compact was recorded. However, sintering and consequent improvement in hardness and wear resistance was effective only up to a certain depth or thickness, depending on the laser parameters. The depth of useful sintering was limited to only about 200–400 μm under that laser sintering.

From above investigation by various authors it can be concluded that amorphous phase formation in binary and multi component alloy system depends not only alloy composition but also the alloying element during MA . The phase formation during present alloy system Al−Si−Ni depends on composition of the alloying element during process of MA.

2.2 Properties and behaviors of bulk metallic glass (BMG)

In addition to the importance to basic sciences, BMGs have some excellent physical and chemical properties which are promising for applications. The mechanical, magnetic and acoustic properties of the BMGs are discussed below.

2.2.1 Mechanical properties

Fig. 2.1 shows the relationship between Young's modulus (E) and tensile fracture strength ($\sigma_{t,f}$) or Vickers hardness (Hv) for typical BMGs [74, 75]. It could be seen that the tensile fracture strength and Hv have a roughly linear relationship with E, which could be expressed as follows: $\sigma_{t,f}$ = 0:002E, and Hv =0:06E/9:8. For vit1, E =90 GPa, $\sigma_{t,f}$ = 1.9 GPa. The slope of 0.002 corresponds to an elastic strain limit of the BMGs. A similar trend was also evident for ordinary crystalline alloys shown in the figure, but the slopes of the linear region for the BMGs were much steeper than that for

the crystalline alloys, indicating the larger elastic limits of the BMGs compared with those of the crystalline alloys [76]. The much better linearity of the lines for BMGs was attributed to the formation of an ideally homogenized solid solution over the whole composition range which was one of the typical features of glassy alloys.

It could be summarized that BMGs have much higher tensile strengths and much lower Young's moduli. The difference in these values between the BMG and crystalline alloys was as large as 60%.The significant difference in the mechanical properties was thought to be a reflection of the difference in the deformation and fracture mechanisms between BMGs and crystalline alloys.

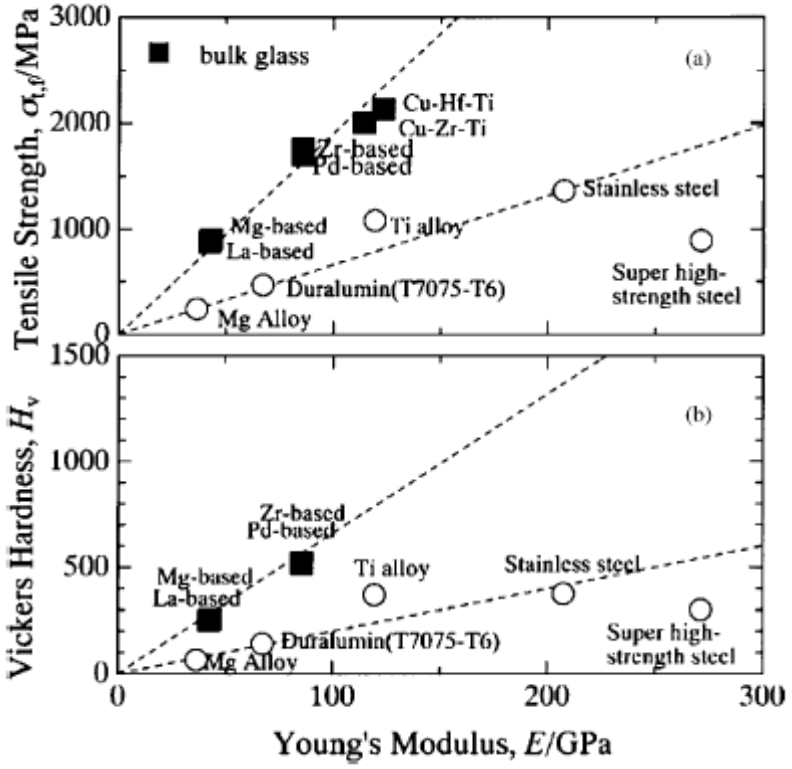

Fig. 2.4: The relations between mechanical properties of typical BMGs: (a) tensile fracture strength (σ_t, f) with Young's modulus (E); (b) Vickers hardness (Hv) with Young's modulus (E) [77]

2.2.2 Acoustic and elastic properties

The experimental data about acoustic and elastic properties in the metallic glasses were scarce, and the vibrational features in the metallic glasses were poorly understood.

Equation of state (EOS) was even more difficult to obtain for the metallic glasses, because the measurements had been impeded mainly by the lack of bulk specimens. A fundamental understanding of microstructural configuration under high pressure in amorphous solids was not as developed as that in crystalline solids. The difficulties in preparing bulk samples were, again, the main obstacle. The BMGs were in the form suitable for measurements of elastic wave propagation. The pressure and temperature dependence of the structural and physical properties of the BMGs could be investigated by the ultrasonic method. In addition to examining the fundamental elastic and thermal behaviors, ultrasonic method was also a powerful tool for studying the relationship of microstructure and properties. Since acoustic property was particularly sensitive to the microstructure, the T-dependent acoustic velocities can provide critical information on the microstructural characteristics and their evolution as well as the elastic and thermal properties during the glass transition of the BMG. The method was a very powerful tool for the study of the nature of glass transition, metallic glassy and supercooled liquid states. Systematic ultrasonic investigation on BMGs had been performed for studying the nature and properties of the metallic glasses and the glass transition [77].

2.2.3 Magnetic properties

The BMGs obtained in multicomponent (Nd, Pr)–Fe-based systems have attracted great attention due to their high coercivity and the absence of glass transition before crystallization in isochronal DSC measurements. The reason for the high coercivity was presumed to be the presence of a relaxed disordered structure that can be regarded as an ensemble of Nd(Pr)–Fe and Nd(Pr)–Fe–Al clusters with large random magnetic anisotropy [79].

The comparison of I–H hysteresis loop of the cast ring-shape Fe-based BMG and similar ring-shape alloy made by stacking the melt-spun ribbons was investigated by Makino et al. [80]. It was observed that the bulk ring-shape alloy has a lower coercive force of 2.2 A/m and much higher initial maximum permeability of 110 000 even in the cast state. The subsequent annealing treatment of the ring-shape sample caused a further increase in initial permeability to 180 000 accompanied by a decrease in coercive to 1.0 A/m. The observation of the domain wall structure indicates that the

much better soft magnetic properties for the as-cast ring-shape BMG are due to the well-arrayed domain wall structure aligned in the circumferential direction. The good high-frequency permeability was due to the combination of low coercivity resulting from the homogeneous glassy structure and low current loss resulting from high electrical resistivity. It was very likely that further improvements to the soft magnetic properties will allow the practical use of BMGs as soft magnetic materials.

2.3 Application of BMGs

With the unique and unconventional characteristics, BMG materials are adopted for application in various fields. One of the great advantages of BMGs is the ease of formation of complicated shapes. Up to now, BMGs have already been used as die materials (Pd–Cu–Ni–P BMG), sporting equipment (ZrTiCuNiBe and ZrTiNiCu BMGs) and electrode materials (PdCuSiP BMG). The development of Fe-based BMGs has reached the final stage for application as soft magnetic materials for common mode choke coils. Success in this area will result in the increasing importance of BMGs in engineering. Table 2.1 summarizes the present and future application potentials for the BMGs.

Table 2.1: possible application field of BMGs

Properties	**Application field**
High strength	Machinery structural materials
High hardness	Cutting materials
High fracture toughness	Die materials
High impact fracture energy	Tool materials
High fatigue strength	Bonding materials
High elastic energy	Sporting good materials
High corrosion resistance	Corrosion resistance materials
High wear resistance	Writing appliance materials
High reflection ratio	Optical precision materials
High hydrogen storage	Hydrogen storage materials
Good soft magnetism	Soft magnetic materials
High frequency permeability	High magnetostrictive materials
Efficient electrode	Electrode materials
High viscous flowability	Composite materials
High acoustic attenuation	Acoustic absorption materials
Self-sharping property	Penetrator
Highwear resistance and manufacturability	Medical device materials

The first step of the new family of materials into the market is the application for making golf plate [81]. In addition to the advantages like low density and high strength-to-weight ratio, other properties such as low elastic modulus and lower vibrational response provide a softer, more firm feel for better control when a golfer strikes the ball. The very less hysteresis loss of BMG means that less energy is absorbed by the club head at impact, so more energy is transferred to the ball. According to the literature of the BMG golf plate manufacturer, steel club heads transfer about 60% of the input energy to the ball and titanium transfers 70%, whereas the metallic glass transfers 99%. With such favorable properties, BMGs are also applied in other high-end sporting goods such as tennis rackets, and may also find applications for baseball bats, bicycle frames, hunting bows, and even edged tools such as axes. A newly developed application utilizing the efficient energy transfer characteristics is the use of BMG

spheres for shot-peening purpose [82]. On the other hand, the possibility of moulding into components with thin sections allows BMG to challenge magnesium alloys in the electronic gadgets market. With the trend of miniaturization of personal electronic devices such as MP3 players and personal digital assistants (PDA), there is an urgent need to make the casing thinner while retaining sufficient mechanical strength. BMGs exhibit apparent advantages over polymeric materials and conventional light alloys. Mobile phones and digital still cameras with BMG casing have already developed.

In addition to sporting goods, the new family of materials could also be promising for other more good applications. Metallic-glass tank-armor penetrator rounds to replace the current depleted uranium penetrators, which are mistrusted of biological toxicity. The high strength and light weight of BMG allows miniaturization and weight reduction in the designs of military components without giving the reliability. Examples are sub-munitions components, thin walled casings and components for electronics and aircraft fasteners.

Another area of commercial interest is a highly biocompatible, non-allergic form of the glassy material that would be suitable for medical components such as prosthetic implants and surgical instruments. The unique properties of BMGs for orthopedic applications include: (1) biocompatible; (2) excellent wear resistance; (3) high strength-to-weight ratio compared to titanium and/or stainless steel; (4) more than twice the strength compared to titanium or stainless steel; (5) possibility of net-shape casting with desirable surface finish. Some of the products taking advantage of these improvements include reconstructive devices, fractured fixations, spinal implants and instrumentation. Another opportunity for medical applications is in the field of ophthalmic surgery, where procedures and instruments are being enhanced to better serve patients in need of cataract surgery.

One of the latest industries attracted by the BMG is the fine jewelry industry. The BMGs can achieve a dazing surface finish which grabs the attention of high-end jewelry makers worldwide. The high-performance characteristics and unique properties of BMG can create a metal surface that is both exceptionally hard and scratch resistant, but can be polished to a high luster that is maintained long time. Also, the ability of

BMGs to be net-shape cast enables jewelry designers to create bold lines and sensual, unique shapes not easily achieved with traditional metals.

In the near future, BMGs materials will become more and more significant for basic research and applications as the science and technology of this new field undergo further development.

CHAPTER 3 Experimental

The present chapter is devoted to presenting the detailed scheme of investigation including the techniques and machines\instruments utilized, and characterization and testing procedures adapted.

3.1 Development of Al-based Amorphous Materials

In the present investigation mechanical alloying was used to develop Al-based amorphous materials.

3.1.1 Mechanical Alloying Route

Pure (> 99.5 wt.%) elemental powders of Al, Si and Ni (purity Ni ≥ 99.8%, Al ≥ 99.7%, Si ≥ 98.5%) having an average particle size < 70 μm were blended under protective atmosphere to obtain the nominal compositions of $Al_{75}Si_{15}Ni_{10}$, $Al_{70}Si_{20}Ni_{10}$, $Al_{65}Si_{25}Ni_{10}$, $Al_{70}Si_{15}Ni_{15}$, $Al_{65}Si_{20}Ni_{15}$, $Al_{78}Si_{14}Ni_{8}$ and $Al_{50}Si_{25}Ni_{25}$. The powder blends were subjected to high energy ball milling in the stainless-steel grinding media at a mill speed of 300 *r.p.m.* by means of a Fritsch Pulverisette high energy planetary ball mill. The ball to powder weight ratio was 10:1, and toluene was used as the process control agent. Milling was done for 50hrs for all compositions. Samples were collected a various instance of milling for tracking the phase formation characteristics during MA.

Figure 3.1: Fritsch Pulverisette-5 planetary ball used for mechanical alloying studies.

3.2 Microstructural Characterization

3.2.1 X-ray Diffraction (XRD)

The identity and phase evolution at different stages of MA were studied by XRD analysis using the Cu K_α (λ=1.542A^o) in a Philips X-pert MPD X-ray diffractometer. X-Ray diffraction patterns were recorded from 20˚ to 100˚ with an accelerating voltage of 40 KV. Data were collected with a counting rate of 3˚/min. The refined values of lattice parameter (*a*) were calculated from the peak positions in the XRD pattern by extrapolation of *a* against ($\cos^2\theta/\sin\theta$) plot to $\cos\theta = 0$. The average crystallite size of Al-rich solid solution was determined from the broadening of Al reflection after stripping of $K\alpha_2$ component by the Philips X'pert Highscore Plus software.which allowed judicious elimination of the contribution due to instrumental and strain effects on the observed peak broadening. For the overlapping peaks, the full-width at half intensity maximum and the true Bragg angle (2θ) were determined by an appropriate

deconvolution exercise. X-ray diffraction of the as milled powder samples were performed using the diffractometer.

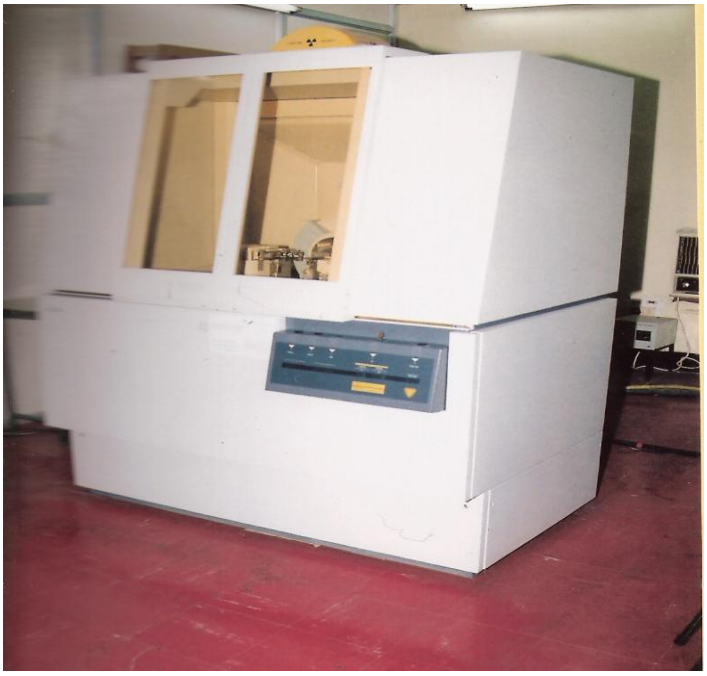

Figure 3.2: Philips X-pert MPD X-ray diffractometer.

3.2.2 Scanning Electron Microscopy (SEM)

A JEOL JSM-6480 LV scanning electron microscope (Fig. 3.4) was used for the morphology, particle size and microstructural characterization of the alloys powder. The images were taken in both secondary electron (SE) and back scattered electron (BSE) mode according to requirement. The composition of the alloys after certain length of MA and extent of stainless-steel contamination in the milled powders, due to the milling media were determined by energy dispersive X-ray (EDX) analysis of selected areas of the specimens using a JEOL JSM-6480 LV EDX attachment, fitted with the scanning electron microscope.

Figure 3.3: JEOL JSM-6480LV scanning electron microscope.

3.2.3 Transmission Electron Microscopy (TEM)

The detailed microstructural characterization and nature of the milled powders of Al-based amorphous powders were carried out using FEI QUANTA (Fig. 3.3) transmission electron microscope. The operating voltage was 200 KV. The samples for TEM analysis have been prepared by mixing the powder with a small amount of pure acetone and stirring for 15 minutes. Two or three drops of the suspension were placed on carbon coated Cu grid and then well dried for 10 minutes before mounting the grid onto the TEM sample holder.

Figure 3.4: FEI QUANTA transmission electron microscope.

3.3 Thermal Stability Study

The thermal stability of the mechanically alloyed powder products was determined by differential scanning calorimetry (DSC) (Perkin Elmer–Pyris Diamond). The powder products were carefully wrapped up in a thin Al foil and then annealed at predetermined temperatures for certain duration under the high purity inert gas (impurity < 10 ppm) atmosphere. Thermal stability of all the compositions was investigated by DSC (STA409C NETZSCH, Germany). The temperature range for all the sample was from room temperature to 500ºC. The heating rate was 10ºC Min^{-1}.

3.4 Fourier transforms infrared radiation (FTIR) spectroscopy

The percentage of transmission was measured by Fourier transforms infrared radiation (FTIR) spectrometer. The sample (pallet) was prepared by mixing small amount of powder with potassium bromide (KBr) and then it was pressed with the hydraulic pressure. The sample was kept in a sample holder of FTIR spectrometer and analyzed to get desired results.

3.5 Nano zeta sizer

The particle size in nanometer range was measured in Nano zeta sizer (Model: Nano ZS, Malvern). The sample was prepared by dispersing small amount of powder in deionized water with constant ultrasonication and magnetic stirring for 30 minutes each. Then the sample was kept in a sample holder with the help of syringe and analyzed to get desired results.

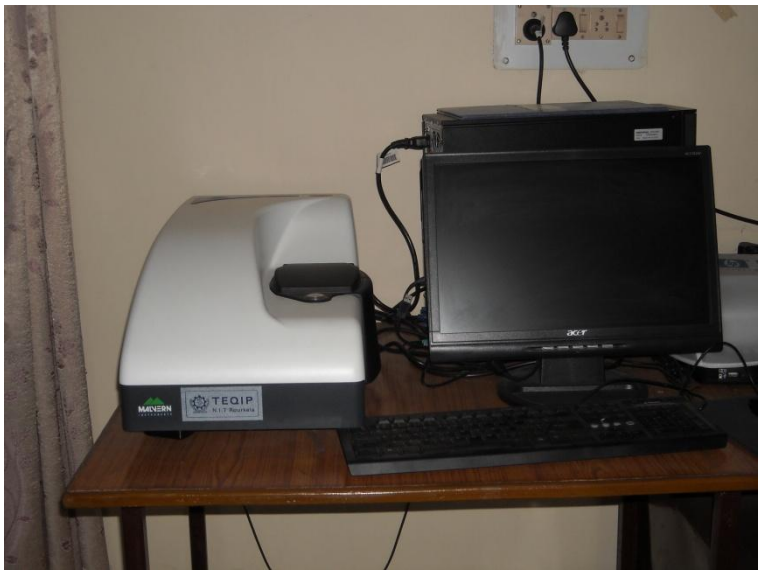

3.5: Nano ZS (Malvern), Nano zeta sizer used in the present study.

CHAPTER 4 Results and Discussion

4.1 MA of Al−Si−Ni Alloys

Rapid solidification processing (RSP) of Al−Si−Ni alloys with different compositions , namely, 14 to 25% Si and 8 to 25% Ni, are known to produce the fully amorphous phase with good bending ductility [11]. Information of the mechanical allying (MA) characteristics of these alloys is not available in the literature . Therefore, the aim of the present work is to develop Al−Si−Ni amorphous phases and /or nanostructures by MA containing 14 to 25% Si and 8 to 25% Ni. For these, the MA characteristics of Al−Si−Ni alloys with various compositions, namely, $Al_{75}Si_{15}Ni_{10}$, $Al_{70}Si_{20}Ni_{10}$, $Al_{65}Si_{25}Ni_{10}$, $Al_{70}Si_{15}Ni_{15}$, $Al_{65}Si_{20}Ni_{15}$, $Al_{78}Si_{14}Ni_{8}$ and $Al_{50}Si_{25}Ni_{25}$ have been analyzed and compared with that of the RSP product of the same composition. The MA was carried out for 50 h for all the compositions under identical conditions.

4.1.1 Morphology of Powdered Samples

Fig 4.1 shows SEM micrographs of $Al_{75}Si_{15}Ni_{10}$ powders after mechanical alloying for (a) 0 h; (b) 5 h; (c) 10 h and (d) 50 h. Before milling, a coarse individual particle can be seen in Fig.4.12 (a). After 5 h of milling, a coarse-layered structure was appeared which may be due to dominating repeated cold welding and less fracturing of the powder particles. After 10 h, a similar type coarse layered structure was observed. The coarse layered structure gradually refined with of milling as fracture predominates cold welding, because of strain hardening of materials. Finally, after 50 h of milling, a finer refined structure was obtained.

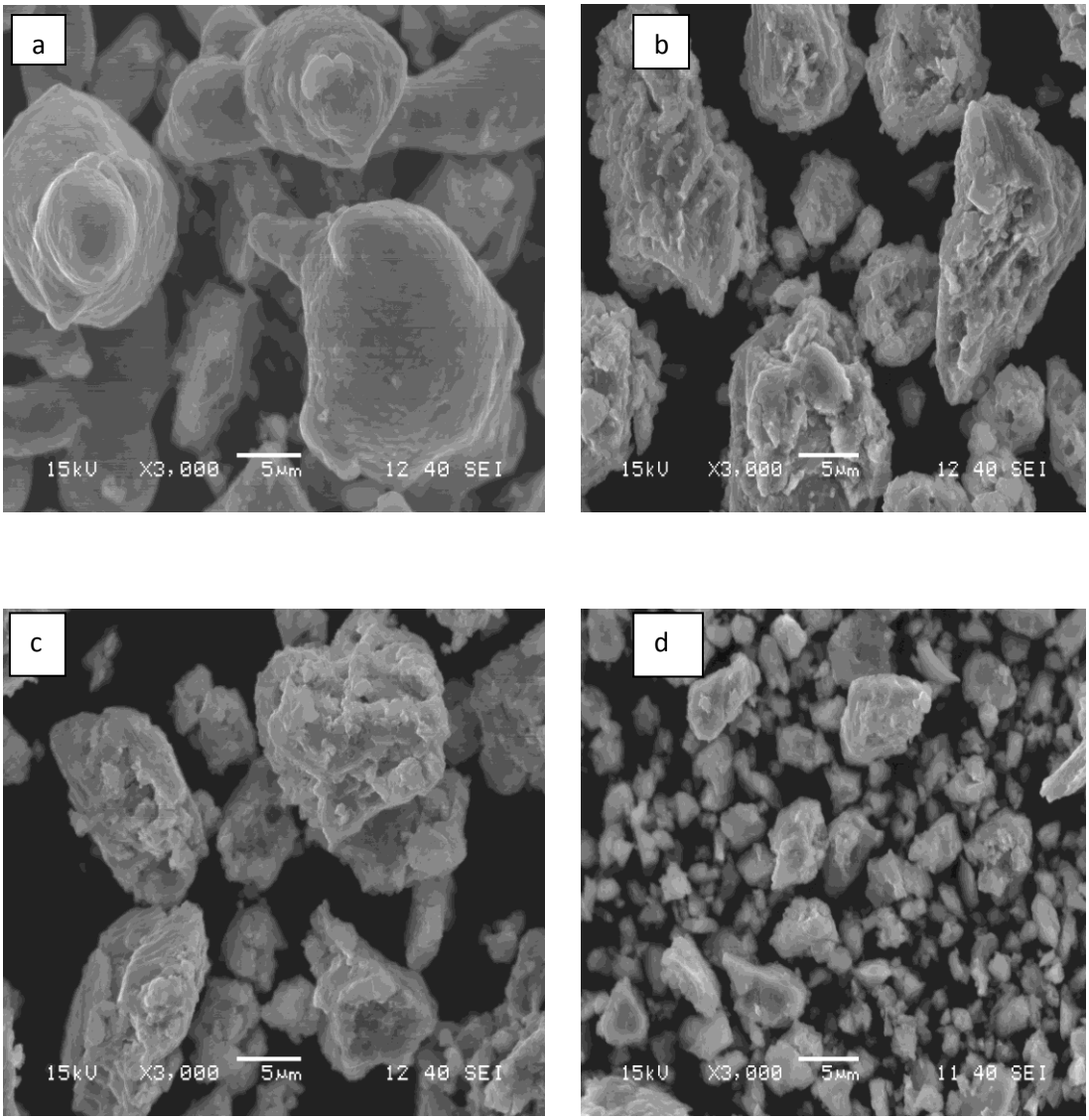

Fig 4.1: SEM images of $Al_{75}Si_{15}Ni_{10}$ powders milled for (a) 0 h; (b) 5h; (c) 10 h and (d) 50 h

The morphology of $Al_{70}Si_{20}Ni_{10}$, $Al_{65}Si_{25}Ni_{10}$ and $Al_{70}Si_{15}Ni_{15}$ milled products is shown in Fig 4.2, Fig 4.3 and Fig. 4.4 respectively. The similar trend of changes in the morphology was observed as explained for $Al_{75}Si_{15}Ni_{10}$.

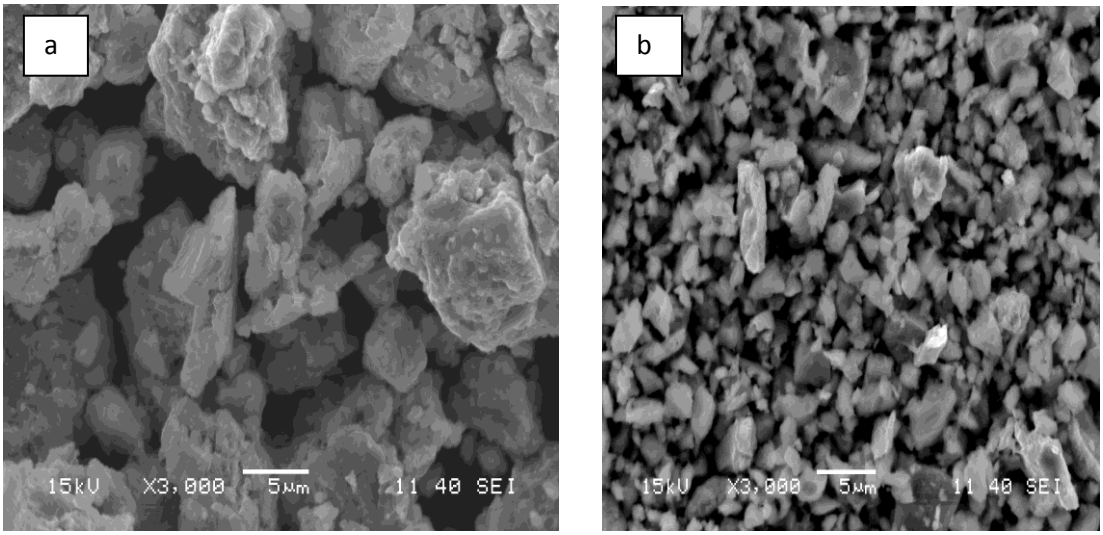

Fig 4.2: SEM images of $Al_{70}Si_{20}Ni_{10}$ powders milled for (a) 10 h and (b) 50 h

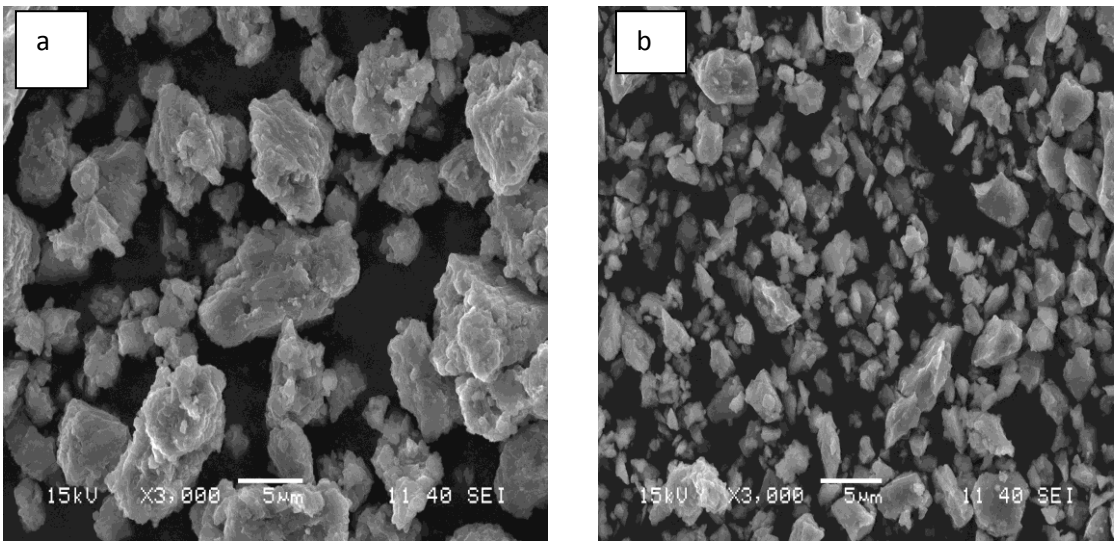

Fig 4.3: SEM images of $Al_{65}Si_{25}Ni_{10}$ powders milled for (a) 10h and (b) 50 h

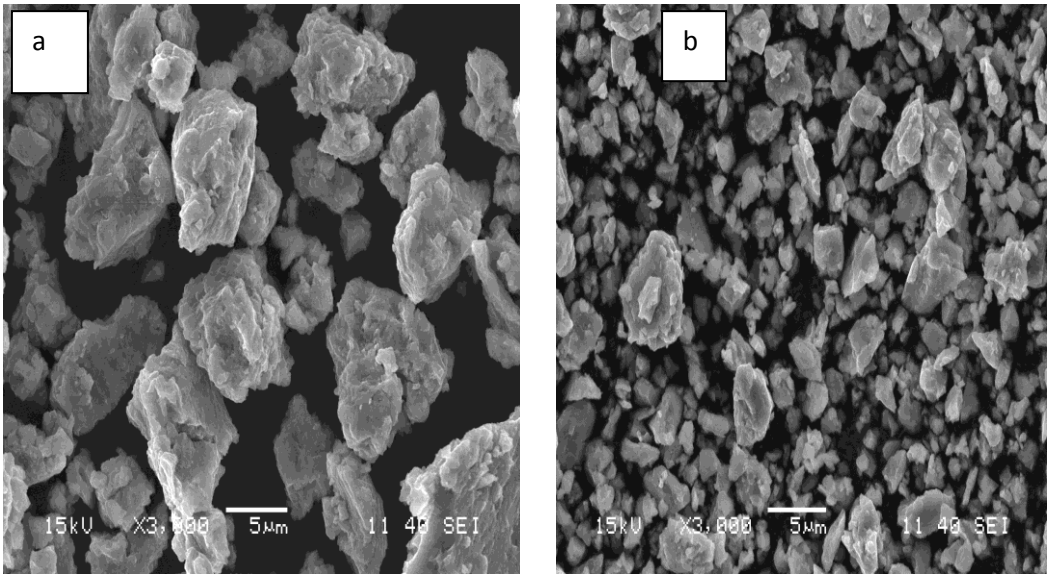

Fig 4.4: SEM images of $Al_{70}Si_{15}Ni_{15}$ powders milled for (a) 10 h and (b) 50 h

4.1.2 Structural Characterization

$Al_{75}Si_{15}Ni_{10}$ Alloy

Fig. 4.5 shows the modulation of the XRD patterns of $Al_{75}Si_{15}Ni_{10}$ composition with the progress of MA up to 50 h of milling. It is interesting to note that Al, Si and Ni peaks were clearly visible during early stage of milling and no intermetallic compound was found during 0-30 h of milling. It is to be noted that the peak intensity gradually decreased and broaden with progress of milling. The peaks corresponding to Ni completely disappeared after 10 h of milling, whereas, Si peaks persisted even after 50 h of MA. Intermetallic phase, Al_3Ni_5, was found to form during the later stage of milling, i.e., 30-50 h. After 50 h of milling the structure appeared to be partially amorphous as evidenced by the presence of a broad amorphous hump in the XRD pattern.

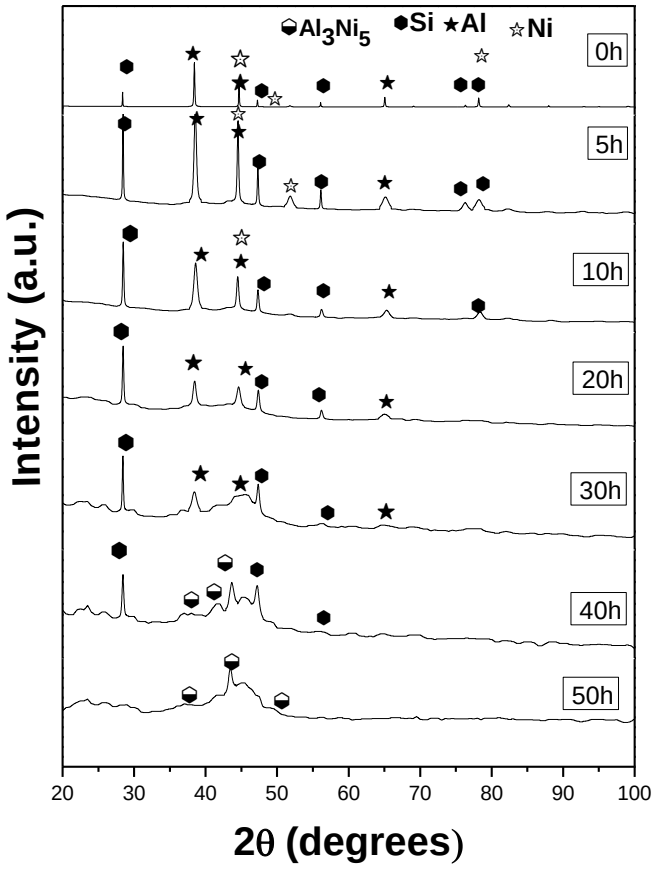

Figure 4.5: Modulation of XRD patterns of $Al_{75}Si_{15}Ni_{10}$ with progress of MA.

$Al_{70}Si_{20}Ni_{10}$, $Al_{65}Si_{25}Ni_{10}$ Alloys

In order to investigate the role of higher at.% of Si in the present alloy system compared to $Al_{75}Si_{15}Ni_{10}$, elemental powder blend containing more amount of Si, *i.e.*, $Al_{70}Si_{20}Ni_{10}$ and $Al_{65}Si_{25}Ni_{10}$, were mechanically alloyed, and the evolution of phases in course of milling was monitored by XRD. Fig. 4.6 shows the modulation of the XRD patterns of $Al_{70}Si_{20}Ni_{10}$ blend with the progress of MA. The phases generated by MA in this case were somewhat different from those found in lower Si containing alloy. Al, Si and Ni, peak was clearly visible during early stage of milling and no intermetallic compound was found during the stage (0-10 h). The peaks corresponding to Ni were completely disappeared after 20 h of milling, whereas, Si peaks were observed after 40

h of milling. Intermetallic compound like Al_3Ni_2 and $Ni_{31}Si_{12}$ was found after 20 h of MA which are gradually disappeared on further milling, and a different set of intermetallic compounds like Al_3Ni and $Al_{0.96}Ni_{1.04}$ appeared after 30 h of MA. No intermetallic was observed after 40 h of milling, whereas, intermetallic phase AlNi was found after 50 h of MA and no Si peak observed after this. After 50 h of milling the structure appeared to be partially amorphous, as evidenced by the presence of a broad amorphous hump in the XRD pattern similar to that of $Al_{75}Si_{15}Ni_{10}$.

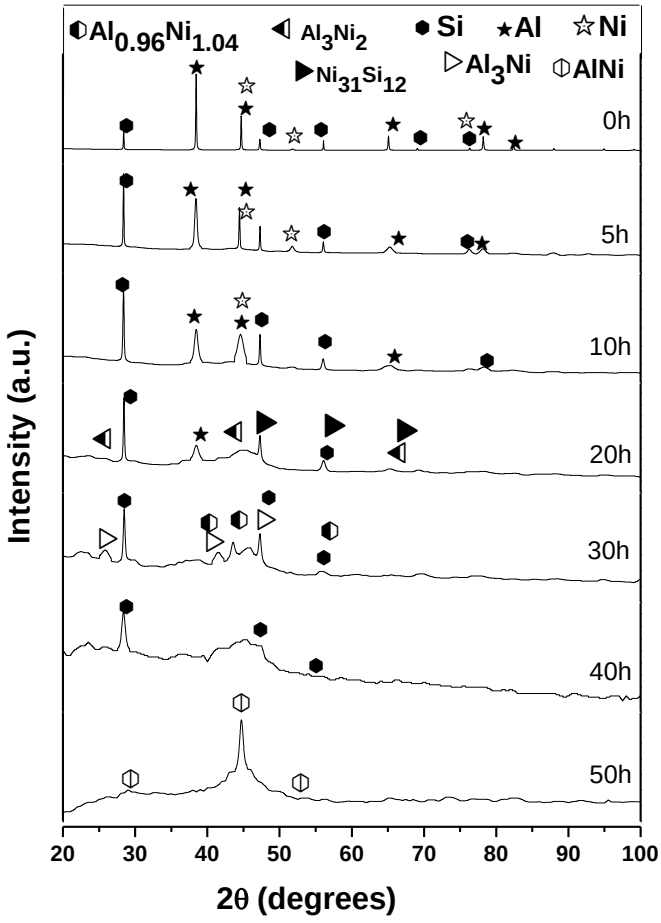

Figure 4.6: Modulation of XRD patterns of $Al_{70}Si_{20}Ni_{10}$ with the progress of MA.

Fig. 4.7 shows modulation of the XRD patterns of $Al_{65}Si_{25}Ni_{10}$ powder blend with progress of MA. Here also, the phases generated by MA were somewhat different from those found in $Al_{75}Si_{15}Ni_{10}$. It was found that Al, Si and Ni peaks were clearly visible during early stage of milling (0-10 h) and no intermetallic compound was found during this stage. The intensity of the peaks decreased and broadened with progress of MA. Intermetallic like Al_3Ni and Al_3Ni_5 appeared to form after 20 h and 30 h of milling, respectively. But, these peaks were completely disappeared after 50 h of MA. A new intermetallic phase $Ni_{31}Si_{12}$, formed after 40 h of milling, disappeared after 50 h of MA. The intermetallic phase obtained after 50 h of milling was Ni_2Al_3. The structure appeared to form a solid solution of Ni and Si with an intermetallic phase of Al and Ni, i.e., Al_3Ni_2.

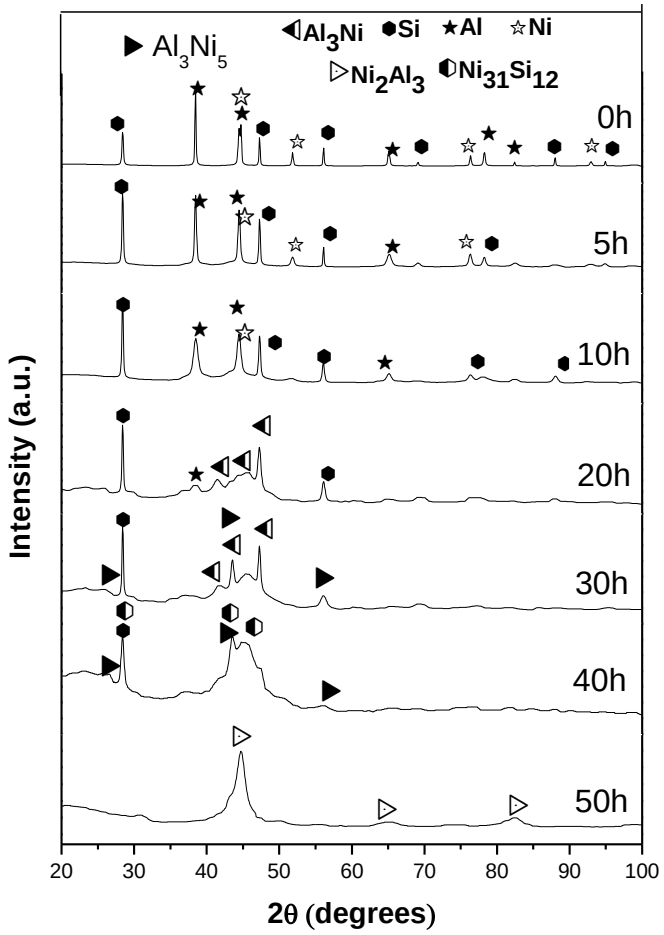

Figure 4.7: Modulation of XRD patterns of $Al_{65}Si_{25}Ni_{10}$ with the progress of MA

$Al_{70}Si_{15}Ni_{15}$ Alloy

In order to observe the role of Ni in the present alloy system, an elemental powder blend containing more amount of Ni, i.e., $Al_{70}Si_{15}Ni_{15}$, compared to $Al_{75}Si_{15}Ni_{10}$, was mechanically alloyed, and the evolution of phases in course of its milling was monitored by XRD as presented in Fig. 4.8. The phases generated by MA in this case were somewhat similar to those found in $Al_{75}Si1_5Ni_{10}$ alloy. The peaks of Al, Si and Ni were clearly visible during early stage (0-10 h) of milling and no intermetallic compound was found during this stage. The intensity of the peaks decreased and broadened with progress of milling as per the characteristics of MA. Intermetallic phase Al_3Ni was formed after 20 h of milling which was completely disappeared after 30 h of milling. New intermetallic phase Al_3Ni_5 was observed after 30 h of milling. After 40 h of milling intermetallic phase Al_3Ni_2 was found to form which remained up to 50 h of milling. The structure appeared to form a solid solution of Ni and Si with an intermetallic phase of Al and Ni, i.e., Al_3Ni_2.

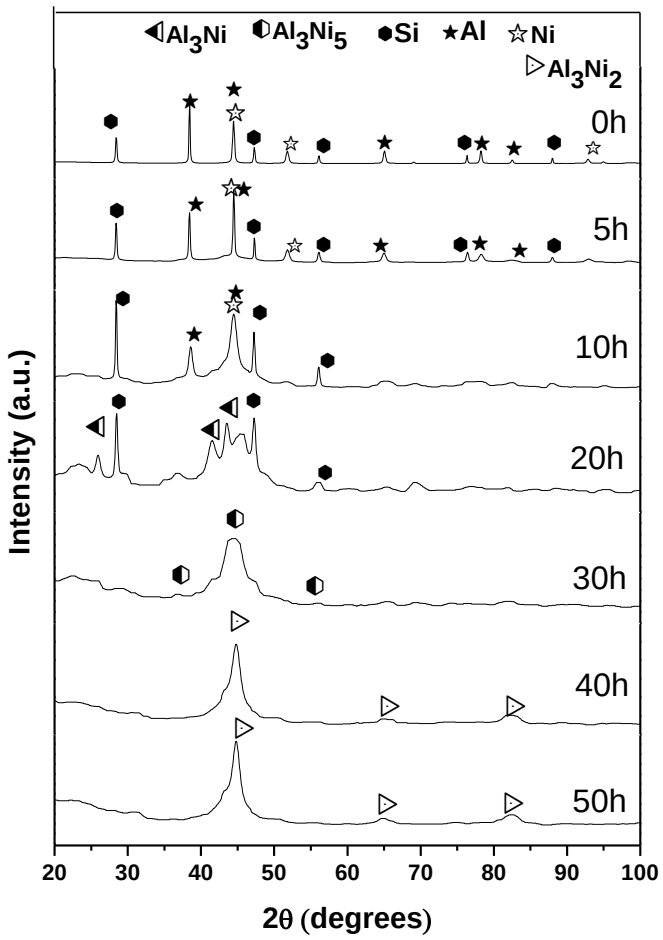

Figure 4.8: Modulation of XRD patterns of $Al_{70}Si_{15}Ni_{15}$ with the progress of MA.

$Al_{65}Si_{20}Ni_{15}$ Alloy

In order to observe the role of Si and Ni, an elemental powder blend containing more amount of Si and Ni, *i.e.*, $Al_{65}Si_{20}Ni_{15}$, compared to $Al_{75}Si_{15}Ni_{10}$, was mechanically alloyed, and the evolution of phases in course of its milling is presented in Fig.4.9. The phases generated by MA in this case were somewhat different from those found in $Al_{75}Si_{15}Ni_{10}$ alloy. New intermetallic phases like $Ni_{31}Si_{12}$, Ni_5Al_3 and $AlNi_5Si_3$ were observed after 20 h of milling and these phases completely disappeared after 40 h of MA. Again new intermetallic phase Ni_3Si was observed after 50 h of milling. After 50 h of milling the structure appeared to be a solid solution similar to $Al_{70}Si_{15}Ni_{15}$.

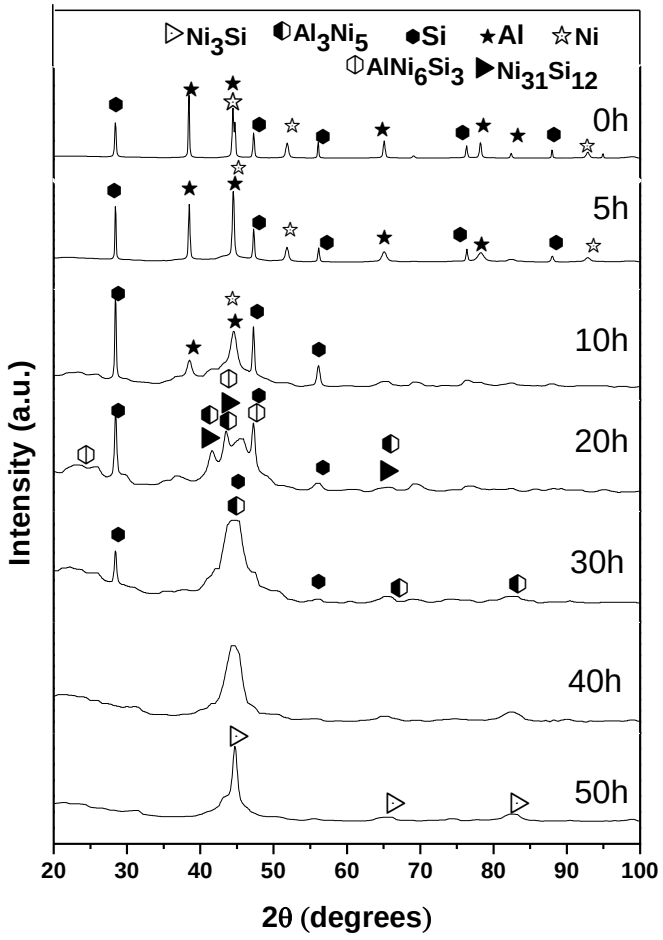

Figure 4.9: Modulation of XRD patterns of $Al_{65}Si_{20}Ni_{15}$ with the progress of MA

$Al_{78}Si_{14}Ni_8$ and $Al_{50}Si_{25}Ni_{25}$ Alloys

Inoue et al. [11] reported the formation of amorphous phase over a wide composition range from about 14 to 25% Si and 8 to 25% Ni by RSP. Keeping this view, the compositions were selected considering minimum and maximum amount of Ni and Si, *i.e.*, $Al_{78}Si_{14}Ni_8$ and $Al_{50}Si_{25}Ni_{25}$. These compositions were also ball-milled for the same duration under identical conditions of milling for the investigation of phase evolution by MA. Figs.4.10 and 4.11 shows modulation of the XRD patterns of $Al_{78}Si_{14}Ni_8$ and $Al_{50}Si_{25}Ni_{25}$ compositions, respectively, with the progress of MA. From Fig. 4.6, it was observed that the peaks of Al, Si and Ni were clearly visible during 0-30

h of milling and no intermetallic compound was formed during this stage which is quite different from other five alloys, discussed above. The peaks corresponding to Si were significantly observed even after 50 h of MA. Intermetallic compounds like Al_3Ni, Ni_5Al_3 and Ni_2Si was observed after 40 h of milling from which Al_3Ni and Ni_2Si were completely disappeared after 50 h of milling. New intermetallic phase $Ni_{31}Si_{12}$ was observed after 50 h of milling. The presence slight amorphous hump and crystalline peaks corresponding to the nanocrystalline intermetallic phases can clearly be noticed in these XRD patterns. It is, therefore, evident that a solid solution with nanocrystalline phases was formed by MA of $Al_{78}Si_{14}Ni_8$.

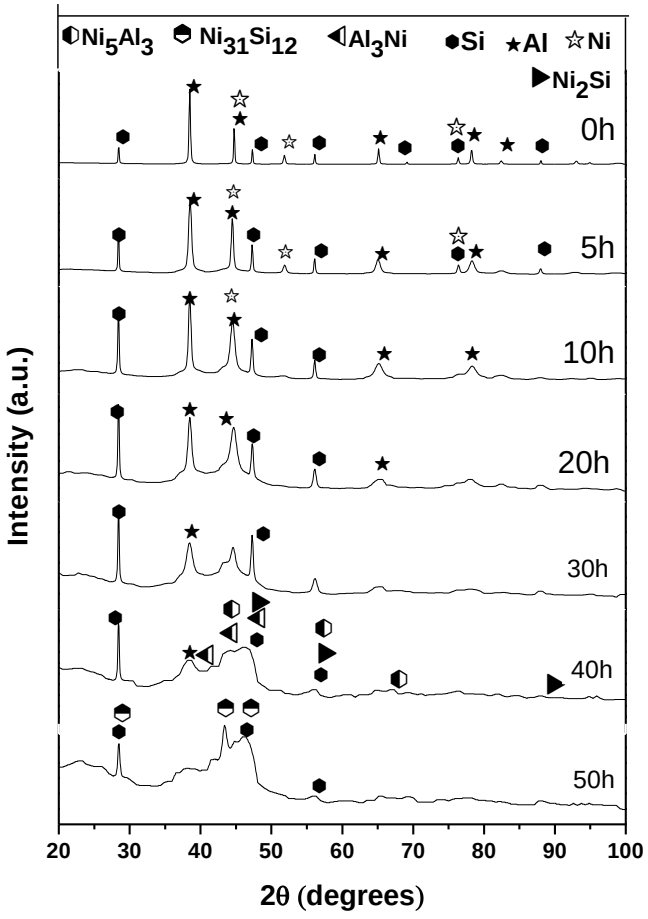

Figure 4.10: Modulation of XRD patterns of $Al_{78}Si_{14}Ni_8$ with the progress of MA

Fig. 4.11 shows modulation of the XRD patterns of $Al_{50}Si_{25}Ni_{25}$ powder blend with the progress of MA. The peaks of Al, Si and Ni, were clearly visible during early stage (0-

10 h) of milling and no intermetallic compound was found during this stage. This is quite different from that of $Al_{78}Si_{14}Ni_8$. Intermetallic phase Ni_2Si was observed after 20 h of milling which was completely disappeared after 30 h. A new intermetallic $Al_{1.1}Ni_{0.9}$ was observed after 40 h of milling, whereas intermetallic like Al_3Ni_5 and Ni_3Si were observed after 50 h of MA. The absence of amorphous hump and the presence of peaks corresponding to the crystalline phases can be clearly noticed from XRD pattern of 50 h milled sample. It is, therefore, evident that a solid solution nanocrystalline phase was formed during MA of $Al_{50}Si_{25}Ni_{25}$.

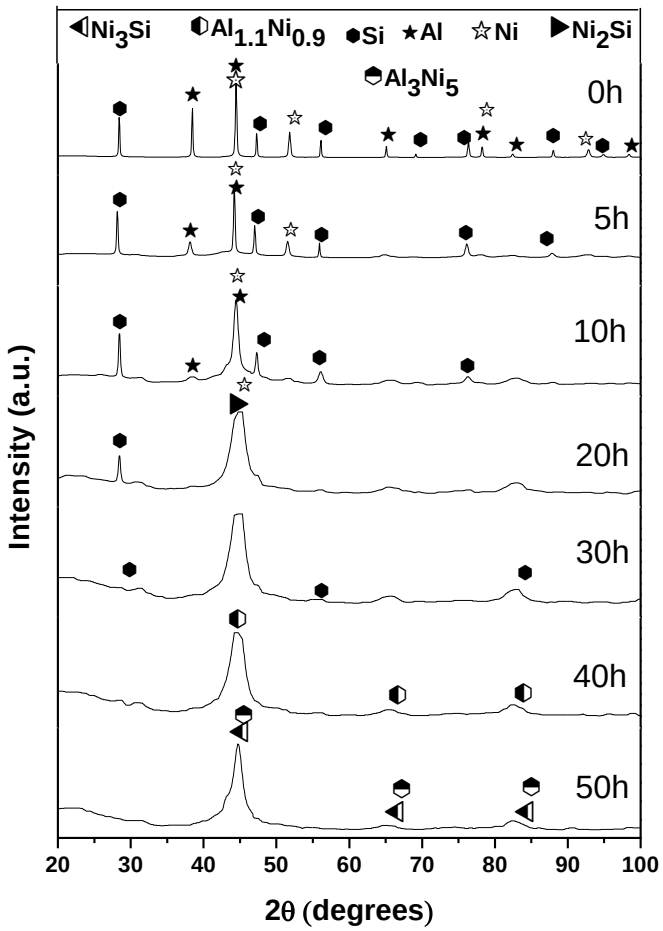

Figure 4.11: Modulation of XRD patterns of $Al_{50}Si_{25}Ni_{25}$ with the progress of MA.

The XRD patterns in Figs. 4.5 and 4.6 indicate that partially amorphous phase were formed by MA of $Al_{75}Si_{15}Ni_{10}$ and $Al_{70}Si_{20}Ni_{10}$ up to 50 h of milling. The other compositions in the present investigation mostly showed the formation of solid solution with intermetallic phase(s).

This result is in conformity with the electron diffraction (ED) patterns of the three alloys in Fig. 4.13, Fig. 4.14 and Fig. 4.15. The ED pattern of 50 h milled sample of $Al_{70}Si_{20}Ni_{10}$ in Fig. 4.13(b) shows a diffused halo due to the presence of amorphous phase, superimposed on the spotty patterns from the crystalline constituents. The ED pattern of $Al_{70}Si_{15}Ni_{15}$ and $Al_{65}Si_{20}Ni_{15}$ alloy milled for the same duration in Fig. 4.14(b) and Fig. 4.15 (b) displays only spotty rings, indicating predominantly crystalline nature of the phases generated in the alloy by MA.

Analysis of the XRD patterns of alloys $Al_{75}Si_{15}Ni_{10,}$ $Al_{70}Si_{20}Ni_{10,}$ $Al_{65}Si_{25}Ni_{10}$, $Al_{70}Si_{15}Ni_{15}$, $Al_{65}Si_{20}Ni_{15}$, $Al_{78}Si_{14}Ni_{8}$ and $Al_{50}Si_{25}Ni_{25}$ alloys revealed that the crystallite size of Al-rich solid solutions initially decreased very rapidly and then gradually decreased to attain almost a constant value for all the compositions. The crystallite size could be in the range of 15-35 nm after 20-30 h of milling (Fig. 4.13). Depending upon the composition the crystallite size refinement during milling is also somewhat different in the intermediate stage, but finally it tends to attain almost a constant value.

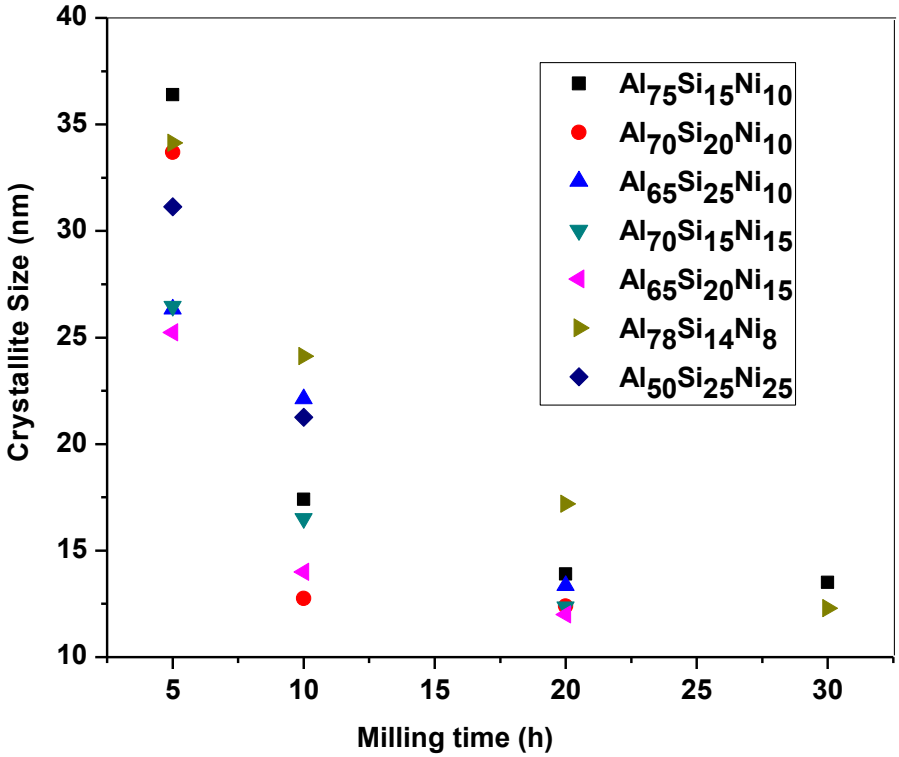

Figure 4.12 Variation of crystallite size of Al-rich solid solution with milling time.

TEM analysis of 50 h milled samples was carried out for $Al_{70}Si_{20}Ni_{10}$, $Al_{70}Si_{15}Ni_{15}$ and $Al_{65}Si_{20}Ni_{15}$ compositions to determine the particle size and crystalline nature of the final products. Figs. 4.13, 14 and 15 display the TEM images and corresponding electron diffraction patterns. Fig.4.13 (a) shows the dark field TEM image and it could be noticed that particle size of the 50 h milled powder is in the range of 20-40 nm. Similarly, from Figs.4.14 (a) and 4.15 (a), it is evident that particle size of the milled products approximately in the same range. This is in reasonable agreement with the average crystallite size of the Al-rich solid solutions estimated by the XRD analysis (Fig. 4.12).

The XRD patterns of 50 h milled samples of $Al_{75}Si_{15}Ni_{10}$ and $Al_{70}Si_{20}Ni_{10}$ composition in Figs.4.5 and 4.6, respectively, revealed that a broad hump is present. This hump is

possibly due to the existence of amorphous phase. To clarify this, selected area electron diffraction (ED) pattern was recorded from 50 h milled sample of $Al_{70}Si_{20}Ni_{10}$ composition and it is presented in Fig.4.13 (b). The diffuse halo in the ED pattern clearly shows the presence of amorphous phase. The ED patterns in Figs.4.14 (b) and 4.15 (b) taken from 50 h milled products of $Al_{70}Si_{15}Ni_{15}$ and $Al_{65}Si_{20}Ni_{15}$ clearly evidenced the presence of crystalline phase(s) as reflected from the spotty patterns. The XRD patterns (Figs.4.8 and 4.9) of the same samples also supporting this results.

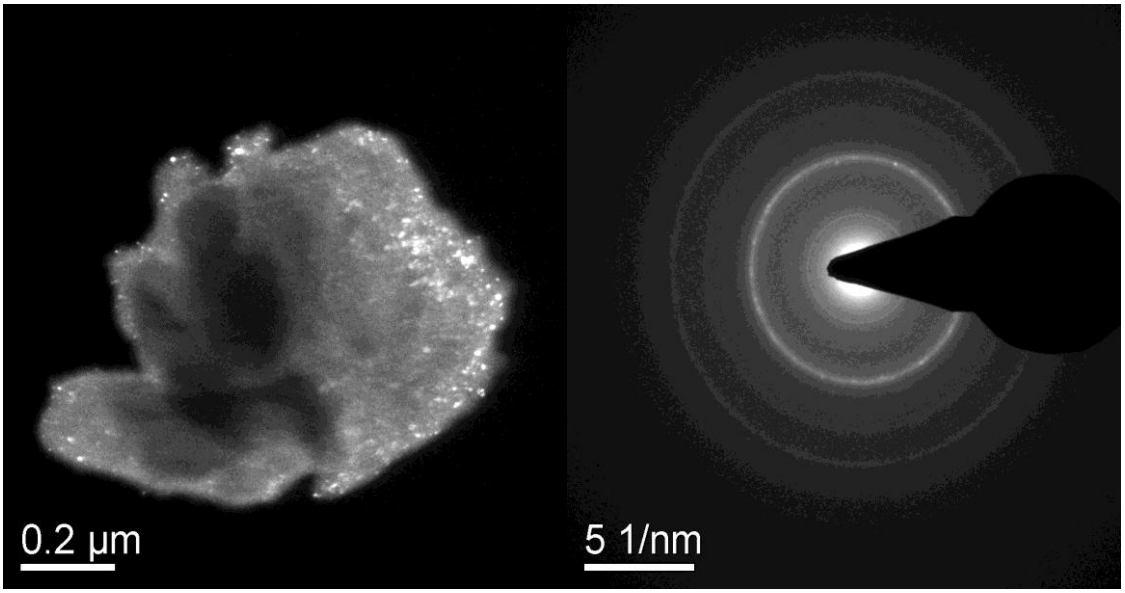

Figure 4.13: (a) Dark field TEM micrographs, and (b) corresponding ED patterns of the as-milled 50 h powders of $Al_{70}Si_{20}Ni_{20}$

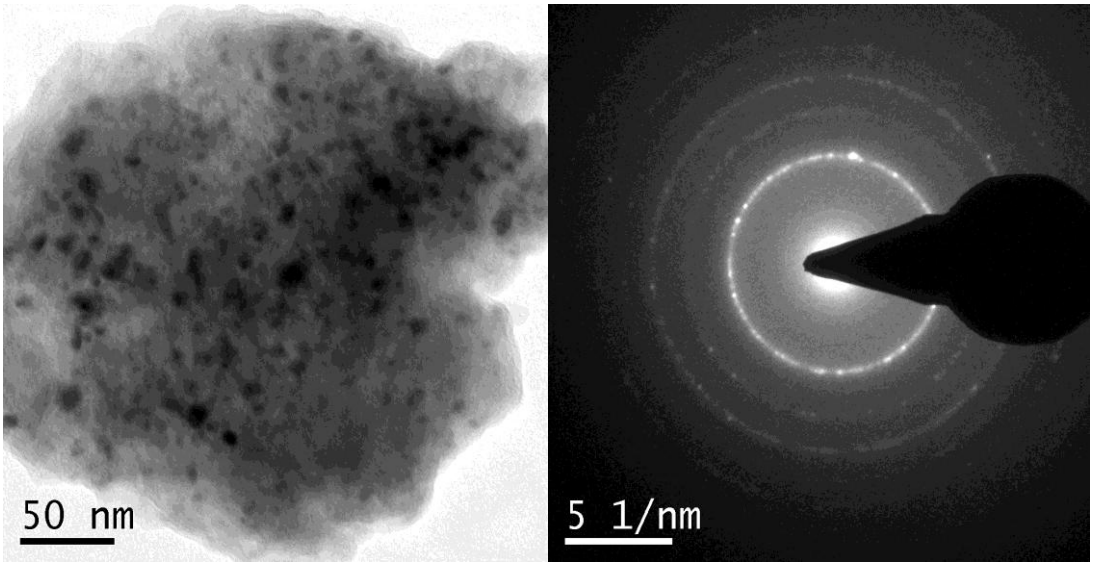

Figure 4.14: (a) Bright field TEM micrographs, and (b) corresponding ED patterns of the as-milled 50 h powders of $Al_{65}Si_{20}Ni_{15}$

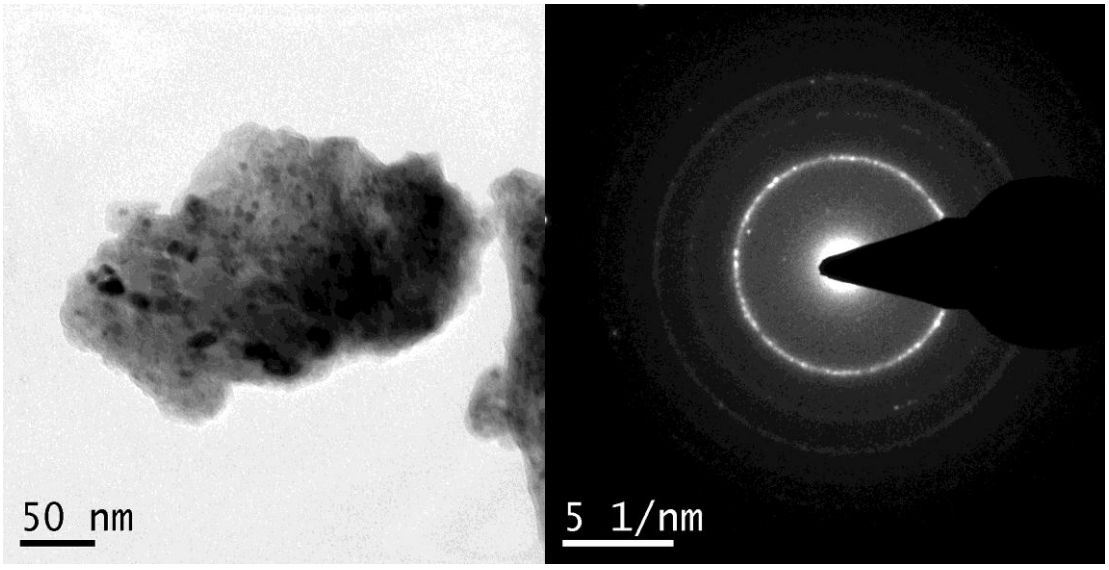

Figure 4.15: (a) Bright field TEM micrographs, and (b) corresponding ED patterns of the as-milled 50 h powders of $Al_{70}Si_{15}Ni_{15}$

In the present study, the lattice microstrain (%) in all the alloys increased rapidly during early hours (0-10 h) of milling and then gradually increased to attain almost a constant

value for all the compositions. The lattice microstrain (%) could be in the range of 0.5-0.6 % after 20-30 h of milling (Fig. 4.16) Thus, Fig. 4.12 along with Fig. 4.16 indicate that the excess energy stored in the milled products in the form of surface energy (due to the crystallite size refinement) and microstrain energy (due to mechanical deformation) in all the alloys is of similar magnitude, and therefore, these factors cannot account for the diversity in structures of the as-milled products in these alloys.

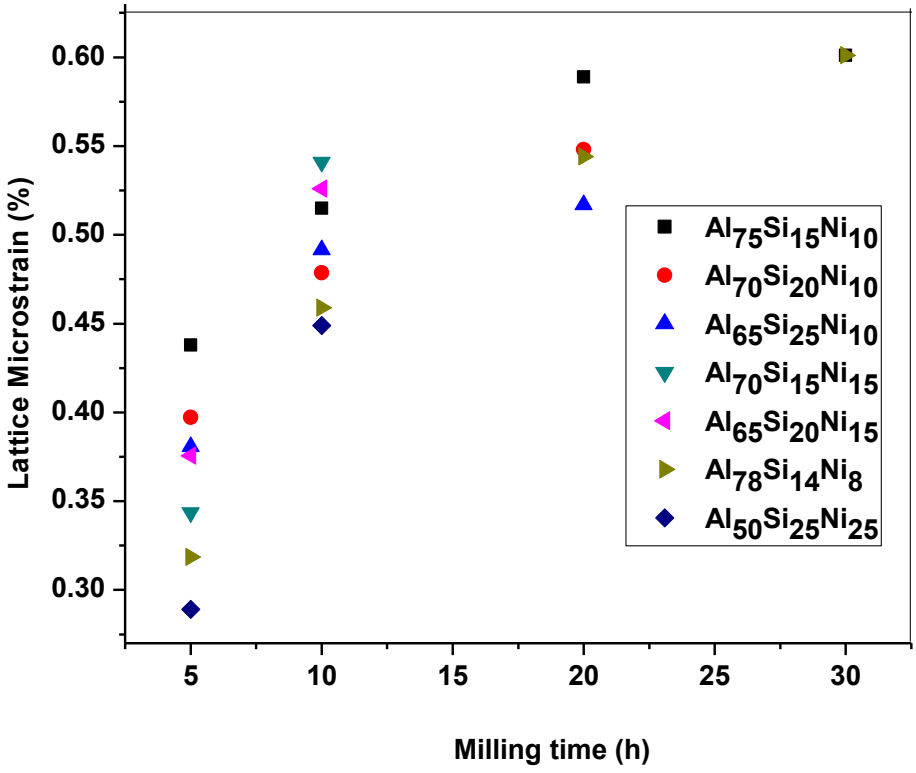

Figure 4.16: Variation of lattice microstrain of Al-rich solid solution with milling time

The variation of lattice parameter of the Al-rich solid solution (a_{Al}) during MA of these alloys is illustrated in Fig. 4.17. It can be noted that the a_{Al} gradually decreased with progress of MA for all the composition. The highest variation of a_{Al} was observed for the compositions of $Al_{75}Si_{15}Ni_{10}$ and $Al_{70}Si_{20}Ni_{10}$, which finally showed the nearly amorphous structures as reflected from XRD pattern (*c.f.* Fig.4.5 and 4.6) and ED

pattern ((*c.f.* Fig.4.13(b)). The lowest variation of a_{Al} was found for the $Al_{78}Si_{14}Ni_8$ and $Al_{50}Si_{25}Ni_{25}$ compositions, which finally formed a crystalline structure with some intermetallic phases (*c.f.* Fig.4.10). Alloys which formed mainly solid solution, i.e., $Al_{65}Si_{25}Ni_{10}$, $Al_{70}Si_{15}Ni_{15}$ and $Al_{65}Si_{20}Ni_{15}$, variation of a_{Al} showed a rapid decrease during milling, but the variation is less compared to that of $Al_{75}Si_{15}Ni_{10}$ and $Al_{70}Si_{20}Ni_{10,}$ i.e., nearly amorphous phase forming compositions, as shown in Fig.4.17. Naturally, the alloying elements, which formed intermetallic compounds, i.e., not entering into the solid solution, do not contribute the lattice parameter variation of the solid solution.

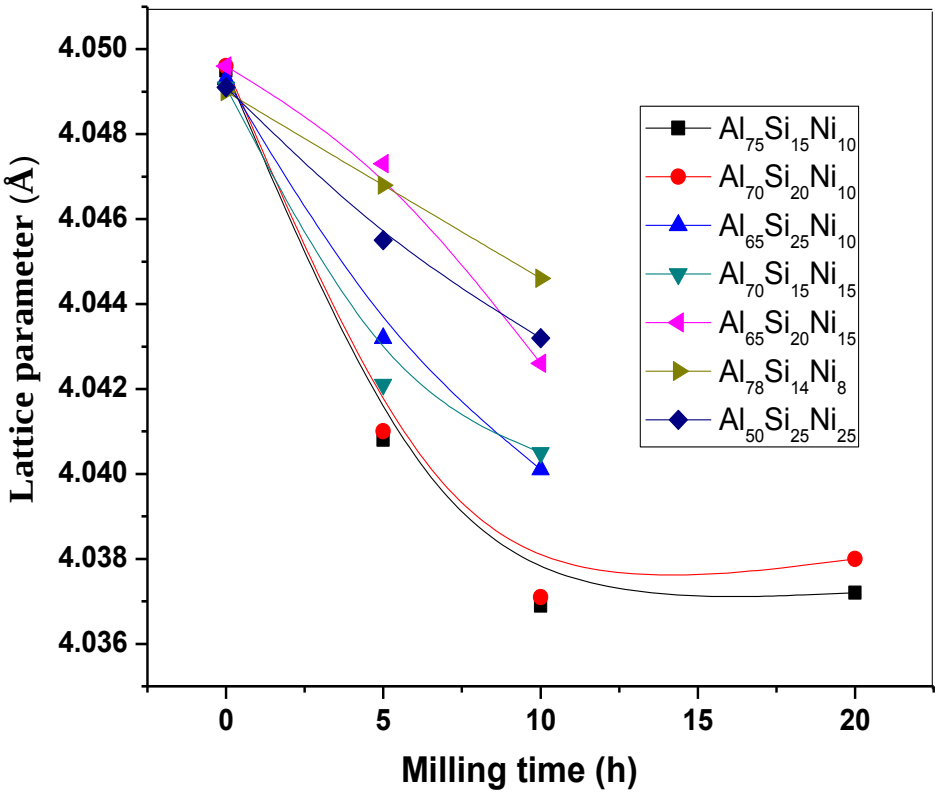

Figure 4.17: Variation of lattice parameter of Al-rich solid solution with milling time.

4.1.3 EDX Analysis

Elemental analysis was carried out in an EDX system attached to scanning electron microscope to investigate the chemical composition of final powder products after 50 h of milling. The EDX analysis results of $Al_{75}Si_{15}Ni_{10}$, $Al_{70}Si_{20}Ni_{10}$, $Al_{65}Si_{25}Ni_{10}$ and $Al_{70}Si_{15}Ni_{15}$ powders after 50 h of milling are shown in Table 4.1, 4.2, 4.3, and 4.4, respectively. A homogeneous chemical composition was attained for all the samples milled for 50 h. This confirms that an alloy formation could be achieved by solid state synthesis.

Table 4.1: EDX analysis of $Al_{75}Si_{15}Ni_{10}$ powder after MA for 50 h

Element	Atomic% Before	Atomic% (After)
Al	75	74.61
Si	15	15.05
Ni	10	10.34

Table 4.2: EDX analysis of $Al_{70}Si_{20}Ni_{10}$ powder after MA for 50 h

Element	Atomic% (Before)	Atomic% (After)
Al	70	70.25
Si	20	20.37
Ni	10	9.38

Table 4.3: EDX analysis of $Al_{65}Si_{25}Ni_{10}$ powder after MA for 50 h

Element	Atomic% (Before)	Atomic% (After)
Al	65	65.42
Si	25	24.11
Ni	10	10.47

Table 4.4: EDX analysis of $Al_{70}Si_{15}Ni_{15}$ powder after MA for 50 h

Element	Atomic% (Before)	Atomic% (After)
Al	70	69.46
Si	15	15.43
Ni	15	15.11

4.1.4 Fourier Transform Infrared (FTIR) Analysis

Fig. 4.18 shows FTIR plot of the $Al_{70}Si_{20}Ni_{10}$ alloy milled for different hours. It is evident from the figure that as the milling h are progressing the percentage (%) of transmittance is getting decreased and percentage (%) of absorbance is getting increased. It is due to the increase in surface area of the particle as the particle size decreased with increase in milling time.

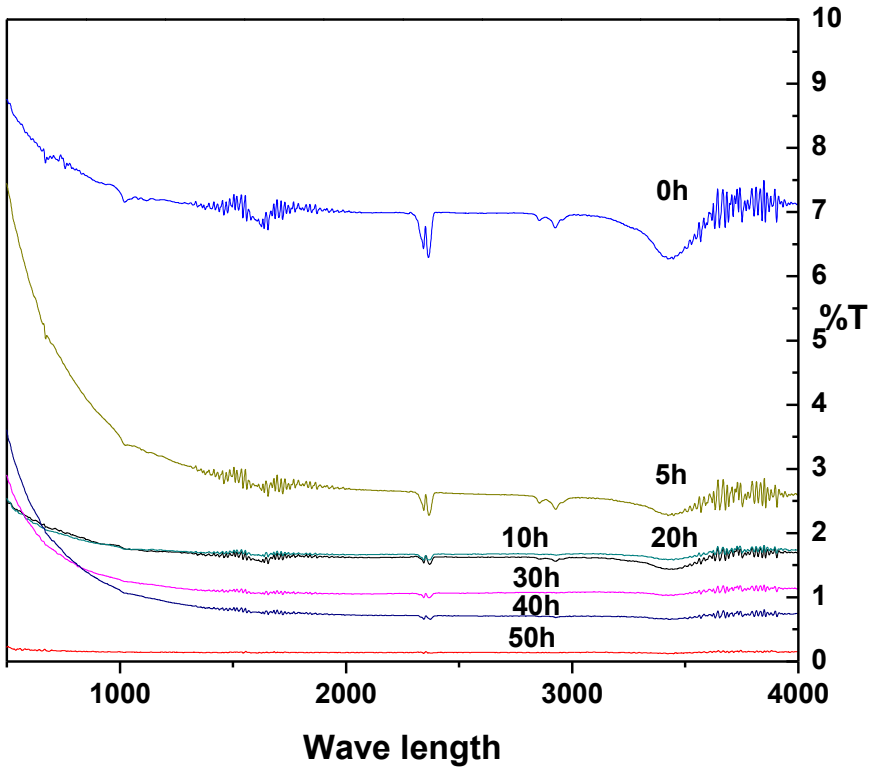

Figure 4.18: FTIR plot of $Al_{70}Si_{20}Ni_{10}$ alloy milled for different hours.

Fig. 4.19 shows the variation of transmittance (%) with crystallite size of the $Al_{70}Si_{20}Ni_{10}$ alloy. It is evident from the fig. that the percentage of transmittance is decreasing with decrease in crystallite size. The crystallite size was calculated from the XRD pattern of this alloy.

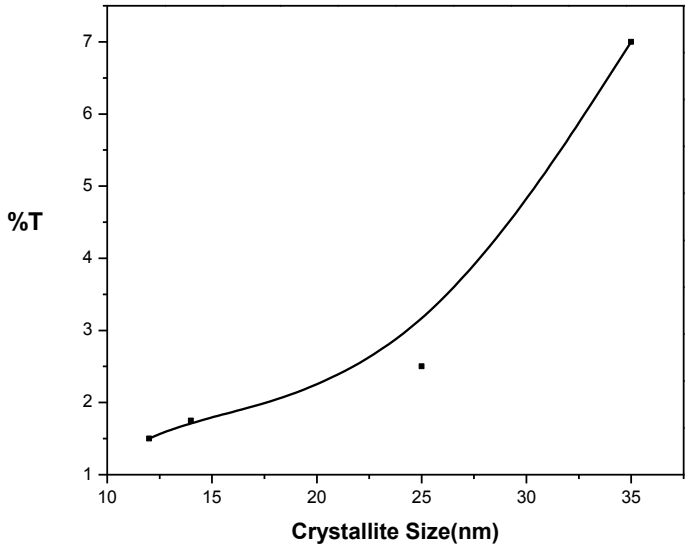

4.19: Transmittance vs. crystallite size plot of $Al_{70}Si_{20}Ni_{10}$ milled powders for different hours.

4.1.5 Particle Size Analysis

Particle size of the milled powder has been measured by nano zeta sizer (NZS). Particle size of the milled powder has been shown in Fig. 4.20 (a) $Al_{75}Si_{15}Ni_{10}$, (b) $Al_{70}Si_{20}Ni_{10}$, (c) $Al_{65}Si_{25}Ni_{10}$, (d) $Al_{65}Si_{20}Ni_{15}$, (e) $Al_{78}Si_{14}Ni_{8}$ and (f) $Al_{50}Si_{25}Ni_{25}$. It is evident from the figure that particle size has been reduced from initial size to the range of 15-40 nm for all alloy composition. The same particle size was also found from TEM micrograph of the same alloy.

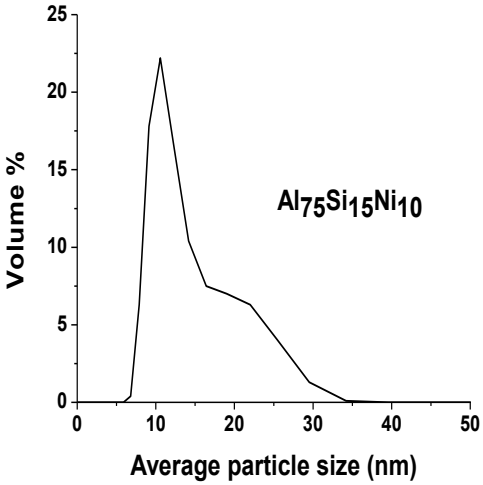
Volume %
Average particle size (nm)
Al75Si15Ni10

(a)

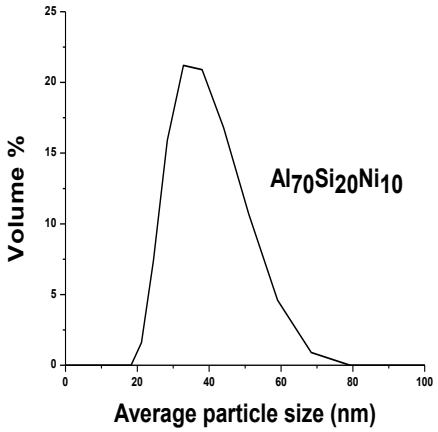
Volume %
Average particle size (nm)
Al70Si20Ni10

(b)

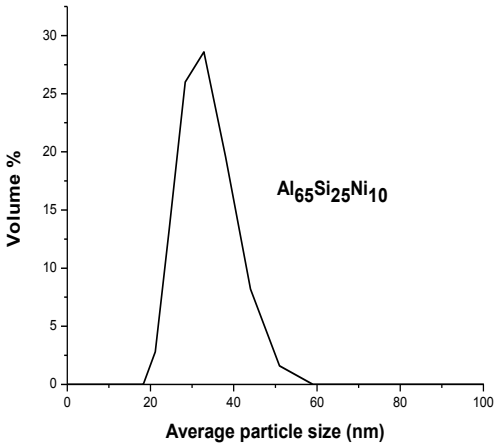
Volume %
Average particle size (nm)
Al65Si25Ni10

(c)

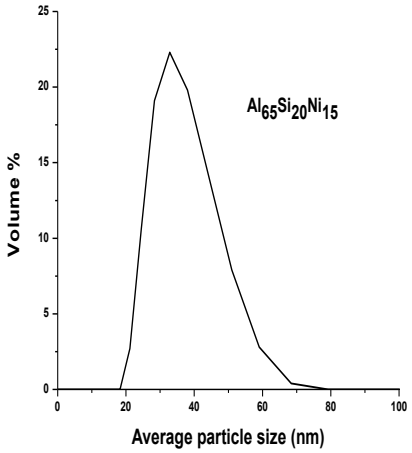
Volume %
Average particle size (nm)
Al65Si20Ni15

(d)

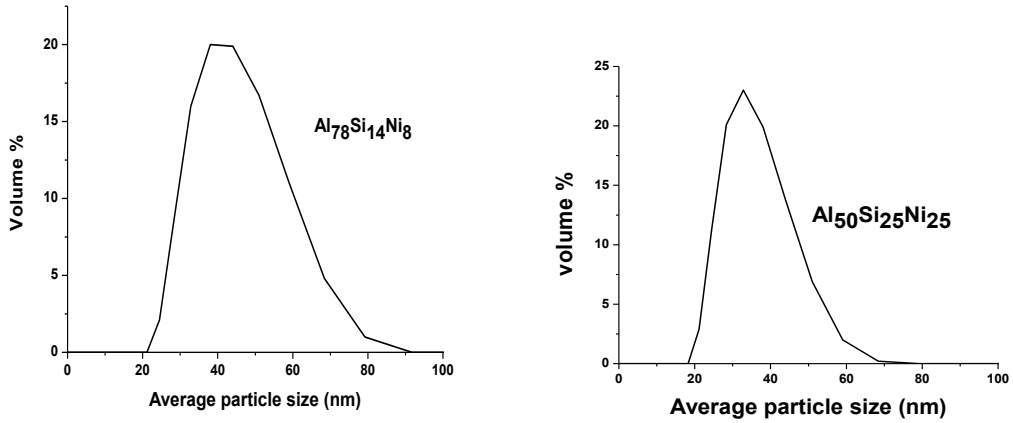

(e) (f)

Figure 4.20: Variation of average particle size with volume % for (a) $Al_{75}Si_{15}Ni_{10}$, (b) $Al_{70}Si_{20}Ni_{10}$, (c) $Al_{65}Si_{25}Ni_{10}$, (d) $Al_{65}Si_{20}Ni_{15}$, (e) $Al_{78}Si_{14}Ni_8$ and (f) $Al_{50}Si_{25}Ni_{25}$ compositions

4.1.6 Thermal Analysis

Fig. 4.21 (a) shows the thermal stability of the 50 h milled Al-rich solid solution of $Al_{65}Si_{20}Ni_{15}$ composition studied by DSC under flowing argon atmosphere. During DSC the temperature was raised up to 300ºC and the heating rate was 10ºC/min. No change of phase was observed during heating up to 300ºC. However, during the temperature rise up to 700ºC (Fig. 22) and the heating rate of 10ºC/min. Glass transition temperature was observed at ~358ºC. Thereafter, four exothermic peaks appeared at ~447ºC (ΔH = 4.369 J/g), ~610ºC (ΔH = - J/mol), ~657ºC and ~672ºC, which were indicative of some phase transformation in the milled product. The detailed study of the phase transformation can be further investigated.

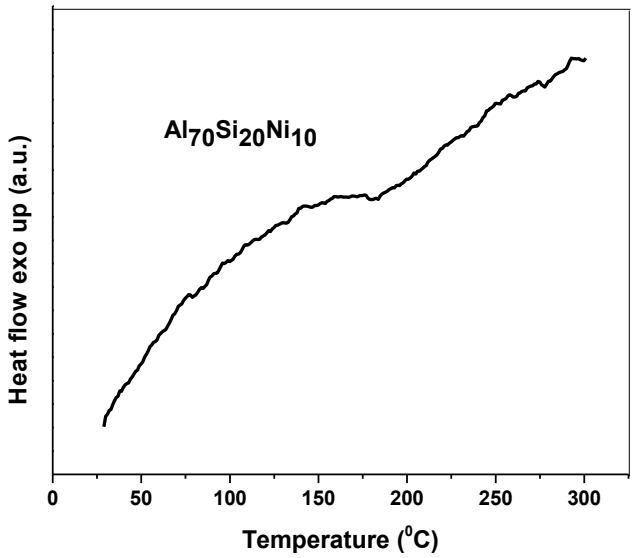

4.21: DSC thermogram of $Al_{70}Si_{20}Ni_{10}$ milled for 50 h up to 300ºC, recorded during heating at a rate of 10ºC/min under flowing argon atmosphere.

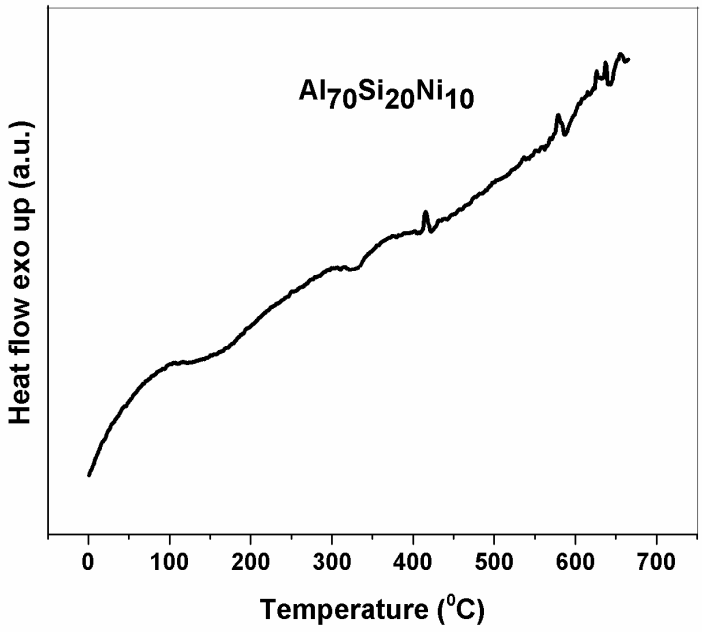

4.22: DSC thermogram of $Al_{70}Si_{20}Ni_{10}$ alloy milled for 50 h up to 700ºC, recorded during heating at a rate of 10ºC/min under flowing argon atmosphere.

4.2 Structure-Property Correlation

In $Al_{75}Si_{15}Ni_{10}$ composition, the intermetallic phases formed in the early stage of MA gradually disappeared and a new set intermetallic compounds formed on further milling. Finally, this alloy formed a partial amorphous phase dispersed with a intermetallic compound of Ni_5Al_3 after 50 h of milling. Similar trend of phase evolution was observed in $Al_{70}Si_{20}Ni_{10}$. But in case of $Al_{65}Si_{25}Ni_{10}$, $Al_{70}Si_{15}Ni_{15}$, $Al_{65}Si_{20}Ni_{15}$, $Al_{78}Si_{14}Ni_8$ and $Al_{50}Si_{25}Ni_{25}$ alloys, a set of intermetallic phases formed during early stage of milling. These intermetallic phases disappeared and a new set of intermetallic compounds formed during (30–50) h of milling, remained after 50 h of milling. Finally, these alloys formed an Al-based solid solution with dispersed intermetallic phase(s) after same duration of MA. New intermetallic phase formed after disappearance of initially formed intermetallic phase which is possibly incapable of sustaining further plastic deformation during milling.

The possible reasons of the phase evolution in the present Al–Si–Ni system by MA could be analyzed in the light of Hume-Rothery rules of alloying [83], the atomic radii of Ni (0.124 nm) and Si (0.117 nm) are smaller than that of Al (0.14318 nm). The atomic size (Ni) difference is within the 15% of the atomic radius of Al. Hence, according to Hume-Rothery's rules; the smaller size Ni atoms are expected to enter into the solid solution of Al during the early stage of MA. Si is also expected to promote solid solution formation as its size also smaller. In some compositions, especially, the high Si containing alloys, i.e., $Al_{65}Si_{25}Ni_{10}$, free Si was observed during the stage of (20–40) h of milling. In some composition it was also found after 50 h of milling, e.g., $Al_{50}Si_{25}Ni_{25}$.

These observations subscribes to the views expressed by Borner [84] that there is a strong correlation between milling condition and phase formation. Continuous milling or milling at speeds of 180 rpm leads to severe sticking of Al to the milling tools causing a shift from the desired stoichiometry to significantly lower Al (about 70 at% Al) and, in turn, higher Y, Ni and Co contents. As a result, Al_2Y, AlY_2 and Al_3Ni_5

intermetallic compounds formed instead of the amorphous phase. In the present alloy system similar effect was observed and intermetallic like Al_3Ni, Al_3Ni_2, Ni_5Al_3, $Al_{1.1}Ni_{0.9}$, $AlNi_6Si_3$ and $Ni_{31}Si_{12}$ was found to form during MA. A similar effect may also be referred for $Al_{85}Ni_5Gd_8$ [85], $Al_{88}Ni_8Co4$ or $(Al_{88}Ni_8Co_4)_{100-x}Zr_x$ with x<3 [86].

The analysis of XRD data for all the compositions showed that variation of crystallite size refinement and accumulation of lattice microstrain energy was almost similar, whereas, variation of lattice parameter of Al-rich solid solution was different. The more pronounced variation of a_{Al} was observed for $Al_{75}Si_{15}Ni_{10}$ and $Al_{70}Si_{20}Ni_{10}$ compositions, which formed nearly amorphous structure after 50 h of MA, as compared to that in $Al_{78}Si_{14}Ni_8$ and $Al_{50}Si_{25}Ni_{25}$, which finally crystalline phases. Whereas, $Al_{65}Si_{25}Ni_{10}$, $Al_{70}Si_{15}Ni_{15}$ and $Al_{65}Si_{20}Ni_{15}$ alloys showed a lattice parameter variation of intermediate range compared to those of partially amorphous forming compositions and crystalline phase forming compositions. These three alloys showed the formation of Al-rich solid solution with dispersed intermetallic phase. Recently, [87] this view was tuned for Al-rich compositions containing more than 80 at.% Al. Therefore, the analysis of the results once again shows that a wide variation in the lattice parameter of the Al-rich solid solution in the course of MA seems to be of profound importance in the design of amorphous forming composition. The evolution of phases and amorphous phase formation could be tuned with ‘confusion principle’ [6], ‘Egami’s criterion’ [88] for the solid state amorphization and the ‘molar volume criterion’ for the glass formation outlined by Rao [89].

It may be recalled that the MA of Al–Si–Ni alloys generated structures, which are different from those reported for RSP of the same compositions [11]. This divergence in the product structures can be analyzed from mechanisms of non-equilibrium phase formation by MA and RSP. In RSP, all the alloying elements are remained in the liquid prior to rapid quenching, and along with these the thermal disorders are frozen-in. Whereas, sequence of dissolution of different alloying elements in the matrix, and the level of mechanical disorders to be introduced can result the phase evolution by MA. The complicated nature and complexity of the MA process and the stability of the

initially formed phases under continued deformation [90, 91] are possibly responsible for the formation of any new phases and/or dissolution of the initially formed intermetallic compounds during further milling. These phenomena finally determine final product structure.

Moreover, several factors are there like kinetic factor, structural factors etc., which possibly control the resultant product. Competition between the amorphization and crystallization, and the extent of the crystallite size refinement and strain energy stored in the milled product during MA possibly play important role in the amorphous phase formation by MA.

4.3 Conclusions

The present investigation on the formation of phases by MA of $Al_{75}Si_{15}Ni_{10}$, $Al_{70}Si_{20}Ni_{10}$, $Al_{65}Si_{25}Ni_{10}$, $Al_{70}Si_{15}Ni_{15}$, $Al_{65}Si_{20}Ni_{15}$, $Al_{78}Si_{14}Ni_{8}$ and $Al_{50}Si_{25}Ni_{25}$, the following conclusions can be made:

(1) The evolution of phase during MA of $Al_{75}Si_{15}Ni_{10}$, $Al_{70}Si_{20}Ni_{10}$, $Al_{65}Si_{25}Ni_{10}$, $Al_{70}Si_{15}Ni_{15}$, $Al_{65}Si_{20}Ni_{15}$, $Al_{78}Si_{14}Ni_{8}$ and $Al_{50}Si_{25}Ni_{25}$ alloys were quite different from RSP of same alloy composition.

(2) Formation of fully amorphous phase was reported in all these alloys by RSP, while partially amorphous phase was observed in $Al_{75}Si_{15}Ni_{10}$, $Al_{70}Si_{20}Ni_{10}$, and Al-rich solid solution formed in $Al_{65}Si_{25}Ni_{10}$, $Al_{70}Si_{15}Ni_{15}$ and $Al_{65}Si_{20}Ni_{15}$ and solid solution with intermetallic phases were formed in $Al_{78}Si_{14}Ni_{8}$ and $Al_{50}Si_{25}Ni_{25}$.

(3) Phase evolution characteristics during MA of $Al_{75}Si_{15}Ni_{10}$ and $Al_{70}Si_{20}Ni_{10}$ alloy were quite different from those in $Al_{65}Si_{25}Ni_{10}$, $Al_{70}Si_{15}Ni_{15}$, $Al_{65}Si_{20}Ni_{15}$, $Al_{78}Si_{14}Ni_{8}$ and $Al_{50}Si_{25}Ni_{25}$. The partial amorphous phase which was obtained in $Al_{75}Si_{15}Ni_{10}$ and $Al_{70}Si_{20}Ni_{10}$ alloys during prolonged milling (50 h) was not found in $Al_{65}Si_{25}Ni_{10}$, $Al_{70}Si_{15}Ni_{15}$, $Al_{65}Si_{20}Ni_{15}$, $Al_{78}Si_{14}Ni_{8}$ and $Al_{50}Si_{25}Ni_{25}$ alloys. The

diffuse halo in the ED pattern from 50 h milled sample of $Al_{70}Si_{20}Ni_{10}$ confirmed amorphous phase formation in it. The ED patterns from 50 h milled products of $Al_{70}Si_{15}Ni_{15}$ and $Al_{65}Si_{20}Ni_{15}$ clearly evidenced the presence of crystalline phase(s) as reflected from the spotty patterns.

(4) The crystallite size was in the range of 15-35 nm for all composition after 20-30 h of milling. Depending upon the composition the crystallite size refinement during milling is also somewhat different in the intermediate stage, but finally it tends to attain almost a constant value.

(5) Lattice microstrain (%) increased to the range of 0.5-0.6 % after 20-30 h of milling. The peaks of Al were observed up to 30 h of milling for $Al_{75}Si_{15}Ni_{10}$ and $Al_{70}Si_{20}Ni_{10}$ alloy which formed partial amorphous phase, whereas, all Al peaks were disappeared after 20 h of milling for all other alloys which formed Al-rich solid solutions.

(6) The more pronounced change in lattice parameter (*aAl*) was observed for alloys which formed partial amorphous phase, whereas, variation of lattice parameter was less for alloys forming Al-rich solid solution or intermetallic compounds.

(7) The layered structure was observed after 10 h of milling in SEM image almost for all compositions.

(8) The decrease in percentage of transmittance with progress of milling time was found for $Al_{65}Si_{20}Ni_{15}$ composition in FTIR analysis. Same can be observed in the plot of crystallite size vs. percentage of transmittance.

(9) The particle size of 50 h milled samples was in the range of 15-40 nm for all the alloys determined through nano zeta sizer analysis. The TEM analysis and crystallite size analysis also corroborated this result.

References

1. Prashanth KG, Scudino S, Murty BS, Eckert J. Crystallization kinetics and consolidation of mechanically alloyed $Al_{70}Y_{16}Ni_{10}Co_4$ glassy powders, Journal of Alloys and Compounds, 477 (2009): pp. 171-177
2. Masumoto T. Recent progress in amorphous metallic materials in Japan, Mater Science and Engineering A 179–180 (1994): pp. 8–16.
3. Inoue A. Amorphous, nanoquasicrystalline and nanocrystalline alloys in Al-based systems, Progress in Materials Science 43 (1998): pp. 365-520
4. Suryanarayana C. Mechanical alloying and Milling, Progress in Materials Science 46 (2001): pp. 1-184
5. Cahn RW. Physical Metallurgy. 3rd edition. Elsevier Science Publishers (1983).
6. Inoue A. Bulk amorphous alloys–preparation and fundamental characteristics. Materials Science Foundation 4, Trans Tech Netherlands, (1998) pp. 1.
7. Revesz A, Vagra L K , Suriach S, Baro M D. J. Mater. Res. 17 (2002) pp. 2140
8. Roy DD, Singh SS, Basu B, Lojkowski W, Mitra R, Manna I. Studies on wear behavior of nano-intermetallic reinforced Al-base amorphous/nanocrystalline matrix in situ composite, Wear, 266 (2009): pp. 1113-1118.
9. Singh SS, Roy D, Mitra R, Subba Rao RV, Dayal RK, Raj Baldev, Manna I. Studies on laser sintering of mechanically alloyed $Al_{50}Ti_{40}Si_{10}$ composite, Materials Science and Engineering: A, 501 (2009): pp. 242-247
10. Azabou M, Khitouni M, Kolsi A. Characterization of nanocrystalline Al-based alloy produced by mechanical milling followed by cold-pressing consolidation Materials Characterization, 60 (2009): PP. 499-505
11. Inoue A, Yamamota M, Kimura H M, Masumoto T. Ductile aluminium-base amorphous alloy with two separate phases, Journal of materials science letter 6 (1987): pp. 194-196.

12. Klement W, Wilens RH, Duwez P. Non-crystalline structure in solidified Gold-Silicon alloys, Nature 187 (1960): pp. 869-870
13. Chen HS. Rep Prog Phys, 43 (1980): pp. 353.
14. Masumoto T. Materials Science of Amorphous Metals, Tokyo: Ohmu, 1982.
15. Schwarz RB. In: Liebermann HH, editor. Rapidly solidified alloys. New York: Marcel Dekker, (1993): pp. 157.
16. Kawamura Y, Kato A, Inoue A, Masumoto T. Int J Powder Metall, (1997): pp. 33-50.
17. Inoue A, Ohtera K, Kita K, Masumoto T. Jpn J Appl Phys, 27 (1988): pp. 2248.
18. Inoue A, Zhang T, Masumoto T. Mater Trans, JIM, 30 (1989): pp. 965.
19. Inoue A, Zhang T, Masumoto T. Mater Trans, JIM, 31 (1990): pp. 177
20. Amiya K, Nishiyama N, Inoue A, Masumoto T. Materials Science Engineering: A, 80 (1994): pp. 692
21. Peker A, Johnson WL. Appl Phys Lett, 63(1993): pp. 2342.
22. Inoue A, Shibata T, Zhang T. Mater Trans, JIM, 36 (1995): pp. 1420.
23. Inoue A, Nishiyama N, Matsuda T. Mater Trans, JIM, 37 (1996): pp. 181
24. Inoue A, Shinohara Y, Gook GS. Mater Trans, JIM, 36(1995): pp. 1427.
25. Inoue A, Zhang T, Itoi T, Takeuchi A. Mater Trans, JIM, 38 (1997): pp. 359
26. Schwarz RB, He Y. Mater Sci Forum; 235-238 (1997): pp. 231.
27. Predecki P, Giessen BC, Grant NJ. Trans Metall Soc AIME, 233 (1965): pp. 1438.
28. Ramachandrarao P, Laridjani M, Cahn RW. Z Metallkd 63 (1972): pp. 43.
29. Davies HA, Hull JB. Scr Metall 6 (1972): pp. 241.
30. Chattopadyay K, Ramachandrarao R, Lele S, Anantharaman TR. In: Grant NJ, Giessen BC,editors. Proceedings of 2nd International Conference on Rapidly Quenched Metals. Cambridge, MA: MIT Press, pp. 157.
31. Furrer P, Warlimont H. Mater Sci Engng, 28 (1977): pp.127.
32. Davies HA. Trans Indian Inst Met, 31 (1981): pp. 292.
33. Inoue A, Ohtera K, Masumoto T. Jpn J Appl Phys, 27 (1988): pp. L736.
34. Inoue A, Ohtera K, Zhang T, Masumoto T. Jpn J Appl Phys, 27 (1988: pp. L1583.
35. Inoue A, Kitamura A, Masumoto T. J Mater Sci, 16(1981): pp. 1895.

36. Suzuki RO, Komatsu Y, Kobayashi KE, Shingu PH. J Mater Sci, 18 (1983): pp. 1195.
37. Tsai AP, Inoue A, Masumoto T. Met Trans 19A (1988): PP. 1369.
38. Inoue A, Ohtera K, Tsai AP, Masumoto T. Jpn J Appl Phys 27 (1988): pp. L280
39. Tsai AP, Inoue A, Masumoto T. J Mater Sci Lett 7(1988): pp.805
40. Davies HA. Amorphous Metallic Alloys Vol. 8. In: Luborsky FE, editor. London, Butterworths, 1983.
41. Massalski TB. Binary alloy phase diagrams, American Society for Metals, Metals Park, OH, 1986.
42. Inoue A, Kato A, Zhang T, Kim SG, Masumoto T. Mater Trans, JIM 32 (1991): pp. 609.
43. Inoue A, Onoue K, Masumoto T. Mater Trans, JIM, 35 (1994): pp. 808.
44. Inoue A, Kita K, Ohtera K, Masumoto T. J Mater Sci Lett., 7 (1988): pp. 1287
45. Di LM, Bakker H. J Phys C: Condens Matter, 3(1991): pp. 3427-32.
46. Harringa JL, Cook BA, Beaudry BJ. J Mater Sci, 27 (1992): pp. 801-804.
47. Kaloshkin SD, Tomlin IA, Andrianov GA, Baldokhin UV, Shelekhov EV. Mater Sci Forum, 235-238 (1997): pp. 565-70.
48. Lai MO, Lu L., Boston, MA: Kluwer Academic Publishers, (1998).
49. Suryanarayana C, Ivanov E, Noufi R, Contreras MA, Moore JJ. J Mater Res, 14 (1999): pp. 377-383
50. Suryanarayana C, Chen G.H., Froes F.H., Scripta Metall Mater 26 (1992): pp. 1727-32.
51. Miki M, Yamasaki T, Ogino Y. Mater Trans Japan Inst Metals, 33 (1992): pp. 839-44
52. Lee CH, Mori M, Fukunaga T, Mizutani U. Japan J Appl Phys 29 (1990): pp. 540-44.
53. Koch C.C., Nanostruct. Mater. 2 (1993): pp. 109-129.
54. Benjamin JS, Volin TE, Met. Trans., 5A (1974): pp. 1929
55. White RL, Ph.D thesis ,Stanford university,1977
56. Koch CC , Cavin OB, McKamey CG, and Scarbrough JO., Appl.phys.Lett., 43 (1983): pp. 1017.
57. Kabayashi KF. J. Materials Science, 25 (1990): pp.1990

58. Abe S. J Japan Inst. Of metals, 8(1990): pp. 1990.
59. Huang B, Tokizane N, Ishihara KN. Journal of Non-Crystalline solid, 117-118 (1990): PP. 688-69.
60. Dong YD. Materials Science and Engineering: A, 134 (1991): pp.867-871.
61. Sherif El-Eskandarany M, Aoki Kiyoshi. Journal of the Less-Common Metals, 169(1991): pp. 235-244
62. Cardellini F, Mazzone G, Vittori Antisar M. Acta Mater., 44 (1996): pp. 1511-1517.
63. Chattopadhyay K, Wang XM, Aoki K, Masurnoto T. Journal of Alloys and Compounds 232 (1996) 224-231
64. Wu NQ, Wu JM, Wang GX, Li ZZ. Journal of Alloys and Compounds 260 (1997): PP. 121-126.
65. Zhou F, Lück R, Scheffer M, Lang D, Lu K. Journal of Non-Crystalline Solids, 250-252 (1999) pp. 704-708
66. Gu X J, Ye F, Zhou F, Lu K. Materials Science and Engineering A, 278 (1999): pp. 61-65
67. Wang Jinhui. Mechanical alloying of amorphous Al–SiO_2 powders, Journal of Alloys and Compounds 456 (2008): pp. 139–142
68. Wilson T W, Choo H, Porter WD, Speakman SA, Fan C, Liaw PK. Amorphization and crystallization processes of the ball-milled Al–Y–Fe–TM alloys (TM = Ni, Co, Cu, and Fe) Journal of Non-Crystalline Solids 352 (2006): pp. 4024–4029
69. Samanta A, Manna I, Chattopadhyay P.P. Phase evolution in Al–Ni–(Ti, Nb, Zr) powderblends by mechanical alloying, Materials Science and Engineering A 464 (2007): pp. 306–314
70. Manna I, Chattopadhyay PP, Banhart F, Fecht H J, Solid state synthesis of amorphous and/or nanocrystalline $Al_{40}Zr_{40}Si_{20}$ alloy by mechanical alloying, Materials Science and Engineering: A, Volume 379 (2004): pp. 360-365
71. Chen H, Cheng X, Zhang J, Ouyang Y, Du Y, Zhong X, Tao X. The compositional range of amorphous phase formation and thermal stability of $Al_{90-x}Fe_5Ni_5Ce_x$, Journal of Alloys and Compounds, 460 (2008): pp. 309-313

72. Zhang DL, Adam G, Ammundsen B. Phase formation during mechanical alloying and subsequent low-temperature heat treatment of Al–27.4at%Fe–28.7at%C powders, Journal of Alloys and Compounds 340 (2002): pp. 226–230
73. Mula S, Ghosh S, Pabi S.K. Synthesis of an Al-based Al–Cr–Co–Ce alloy by mechanical alloying and its thermal stability, Materials Science and Engineering: A 472 (2008): pp. 208–213
74. Inoue A, Zhang T, Takeuchi A. Appl. Phys. Lett. 71 (1997): pp. 464
75. Inoue A, Zhang W, Zhang T, Kurosaka K.. High-strength Cu-based bulk glassy alloys in Cu–Zr–Ti and Cu–Hf–Ti ternary systems, Acta Mater. 49 (2001): pp. 2645.
76. Schuh CA, Nieh TG. Acta Mater. 51 (2003): pp. 87.
77. Wen P, Wang RJ, Pan MX, Zhao DQ, Wang WH. J. Appl. Phys. 93 (2003): pp. 759.
78. Wei BC, Loser W, Xia L, Roth S, Pan MX, Wang WH, Eckert J, Acta Mater. 50 (2002): pp. 4357.
79. Wei BC, Wang WH, Pan MX, Han BS. Phys. Rev. B 64 (2001): pp. 012406.
80. Makino A, Inoue A, Mizushima T. Mater. Trans. JIM 41 (2000): pp. 1471.
81. Johnson WL. MRS Bull. 24 (1999): pp. 42.
82. Inoue A, Shen BL, Zhang W, in: Proceedings of the Third International Conference on Bulk Metallic Glasses, Beijing, October 2003.Raghavan V. (1992).
83. Physical Metallurgy: Principles and Practice, Prentice-Hall of India Private Limited, Fifth printing, New Delhi. (2006): pp 1–258.
84. Borner I, Eckert J. Phase transformartion and properties of mechanically alloyed amorphous $Al_{85}Y_8Ni_5Co_2$, Scripta Materialia 45 (2001): pp. 237-244.
85. Benameur T, Inoue A. Mater Trans JIM, 36 (1995): PP. 240
86. Benameur T, Inoue A, Masumoto T. Mater Trans JIM, 35 (1994): PP.451
87. Mula S, Ghosh S, Pabi SK. On the formation of phases by mechanical alloying and their thermal stability in Al–Mn–Ce system, Powder Technology, 191(2009): pp. 176-181
88. Egami T. Universal criterion for metallic glass formation. Mater Sci Eng A 226–228(1997): pp.261–267.

89. Rao PR.. On glass formation in metal–metal systems. Z Metallkd 71 (1980): pp.172–177.
90. Pabi SK, Das D, Mahapatra TK, Manna I. Mathematical modelling of the mechanical alloying kinetics. Acta Mater 46 (1998): pp. 350–3510.
91. Das D, Chatterjee PP, Manna I, Pabi SK. A measure of enhanced diffusion kinetics in mechanical alloying of Cu-18 at.% Al by planetary ball milling. Scripta Mater 41 (1999): pp. 861–866.